UNIVERSIDADE DA BEIRA INTERIOR
Engenharia

Modeling of Spray/Wall Interactions: Based on Droplet Morphology Dynamics

(versão corrigida após defesa)

Rúben Filipe Torres Ribeiro

Dissertação para obtenção do Grau de Mestre em
Engenharia Aeronáutica
(ciclo de estudos integrado)

Orientador: Prof. Doutor André Resende Rodrigues da Silva

Covilhã, maio de 2019

Acknowledgments

I would like to take this opportunity to express my gratitude to Professor André Resende Rodrigues da Silva, for his guidance and cientific support offered during the duration of this dissertation.
Obviously, i also want to thank my family, especially my sister and parents, for this achievement is also theirs. Last, but not least, i am grateful to Joana for her encouragement and patience during this key period of my academic life.

Resumo

O presente trabalho tem como objetivo aperfeiçoar o conhecimento relativo ao impacto de sprays, que é de extrema importância para a otimização de uma variedade de áreas de investigação, tais como sistemas de combustão, processos de coating ou até de arrefecimento, e também emissões de diversos poluentes. Esta última área de investigação referida tem vindo a ganhar cada vez mais relevância devido a óbvias preocupações ambientais que enfrentamos em pleno século vinte e um. Ao longo deste trabalho, o nosso *in-house code* foi adaptado para aplicar as condições de fronteira e tratamento de atomização secondária propostas por Ma et al. [41]. As complexas relações entre o spray incidente e a correspondente superfície de impacto ainda estão longe de estarem devidamente elucidadas, pelo que este trabalho visa aproximar-nos desse objetivo. Foi também, evidentemente, realizada uma extensa revisão bibliográfica relativa a todas as diferentes facetas deste trabalho, ou seja, tanto ao campo teórico como ao computacional. Existem na literatura diversos modelos computacionais que pretendem retratar a relação entre o spray projetado e a superfície de impacto. Contudo, existe também uma clara impossibilidade física de reproduzir todas as condições possíveis desse mesmo impacto, o que torna todo o tipo de adição a este contexto extremamente útil.

Um dos primeiros modelos a emergir foi proposto por Naber e Reitz, pelo que utilizava um código KIVA, e propunha um único critério de transição para determinar se ocorria ou não *splash*. À primeira vista, este modelo apresentava limitações claras uma vez que não contabilizava as condições de ocorrência de cada regime de impacto. Anos mais tarde, Senda apresentou um modelo que permitia prever não só atomização secondária e a formação de *liquid film* resultante do impacto, mas também o processo de transferência de calor resultante deste processo. Este modelo proposto por Senda, apresentava resultados relativamente precisos, contudo carecia de adaptabilidade, algo que limitava o seu leque de aplicação gravemente. Bai e Gosman, utilizando o modelo $\kappa - \varepsilon$ para a fase de gás e um método estocástico Lagrangiano para a fase de *spray*, tentaram preencher a falta de aplicabilidade do modelo de Senda, através da introdução de de novos regimes e da modelação das condições da parede. Os resultados traduziram-se em melhorias no que toca à descrição das gotas secondárias, principalmente através da utilização de uma distribuição qui-quadrado, e da inclusão de energia de superfície e dissipação de *film* nas equações de conservação. Apesar destes esforços, também este modelo não conseguiu vingar amplamente.

Tendo em conta alguma alterações que emergiram de literatura recente, foram utilizados parâmetros como a temperatura de saturação e altura do filme de líquido para estabelecer condições de fronteira mais pormenorizadas e precisas que representassem fielmente um mais alargado leque de situações. Estas alterações de condições de fronteira, juntamente com a adição de novas equações representativas da conservação de massa e energia, permitiram que se tratassem as gotas secundárias como uma coroa em formação e posterior *rim*. Este trabalho permite obter uma análise pormenorizada aos resultados obtidos, pelo que há um claro foco de análise no que respeita às propriedades das gotas secundárias. No que toca a este assunto, um novo regime relativo às propriedades das gotas secundárias foi inserido e denominado ”região incerta”. Este quantifica a probabilidade de ocorrer splash ou ressalto mediante uma distribuição gaussiana, uma vez que a quantidade de informação disponível para estas condições de aplicação é escassa.

Este trabalho permite, igualmente, estabelecer uma clara distinção entre *corona* e *prompt splash*, o que acrescenta uma quantidade de condições reprodutíveis considerável ao nosso

código *in-house*.

Palavras-chave

Impacto de gotas, filme de líquido, leidenfrost , corona splash , prompt splash, ressalto , impacto de spray, superfície quente.

Abstract

The present work has the objective of perfecting our knowledge related to spray impact, which is of paramount importance for the optimization of a wide variety of investigation areas, such as combustion systems, coating and cooling processes, and also pollutant emissions. This last referred area has been gaining more and more importance due to the obvious environmental concerns that we face in our age. For these reasons,a remarkable effort by the scientific community has been made in order to deepen the understanding of the mechanisms underlying the spray impingement process. In this dissertation, and through numerical analysis, our in-house code was adapted to reflect the impingement conditions and secondary atomization treatment proposed by Ma et al. [41]. The complex relations between incident spray and the corresponding impact surface are yet far from being duly elucidated, whereby this paper aims to bring us closer to that objective. Evidently, an extensive bibliographic review was performed about theoretical and computational concepts. There are numerous computational models in literature that intend to portray the relation between the impinging spray and the impact surface. Although, not all of these models display the complexity necessary to represent different types of conditions, such as the presence of liquid film or even the existence of a temperature so high that prevents the contact between spray and wall through the generation of a vapor layer. This phenomenon is commonly known as "Leidenfrost effect" and is usually neglected. One of the first to emerge was proposed by Naber and Reitz, employing the KIVA code, and proposed a single threshold to determine if splash occurred or not. At first glimpse, this model was obviously flawed by way of not accounting for the conditions of occurrence of each impingement regime. Later on, Senda presented a model of their own that was able to predict not only secondary atomization and liquid film formation resulting from the impinging droplets, but also the heat transfer process present in such situation. Sendas's model despite presenting moderate accuracy, lacked the adaptability to a wider spectrum of applications. Bai and Gosman, using the $\kappa - \varepsilon$ model for the gas phase and a stochastic Lagrangian method for the spray, tried to solve this lack of adaptability by modelling the effect of wall conditions and introducing several new regimes. The results translated in improvements describing the secondary droplets, mainly through fitting secondary droplets in a chi-squared distribution and by including surface energy and film dissipation in the conservation equations. Despite these satisfactory results, this model also failed to attain general applicability.

Taking into account recent literature alterations, parameters such as saturation temperature and liquid film thickness were utilized to establish more detailed boundary conditions with the intent to represent a more extended range of possible scenarios.

In the application of this model a distinction was made between corona splash and prompt splash due to the fact that secondary droplets present different characteristics for each case. Questions such as expansion of the lamella, crown formation and propagation, as well as splashed film mass or transformed mass from crown to secondary droplets became of paramount importance during all the stages of the identified regime and were all detailed in this model.

The size and velocity of secondary droplets depend strongly on the initial conditions of the spray at the injector exit, as well as the interaction between incident droplets, crossflow, liquid film, evaporation rate, and interposed hot wall. All these parameters are considered in this macroscopic model of the spray/wall interactions.

This dissertation allows us to obtain a detailed analysis about the properties of secondary droplets. In what concerns this subject, a new regime was implemented to a specific gap of

boundary conditions and denominated ”uncertain region”. This regime quantifies the probability of splash or rebound occurrence through a uniform distribution since the available information for these conditions is very scarce. Moreover, simulations are carried out for predicting the outcome of flows, including liquid film formation, droplet breakup, and spray evaporation. The numerical results are then compared against experimental data available in open literature to ascertain the predictions capabilities and validate the model.

Keywords

Droplet impact, liquid film, leidenfrost, rebound, corona splash, prompt splash, spray impingement, hot wall.

Contents

List of Figures

List of Tables

Nomenclature

ρ	kg/m^3	Density
D	m	Diameter of the drop
C_D	-	Drag coefficient
R	m	Drop radius
θ	[°]	Dynamic contact angle
μ	$kg/m/s$	Dynamic viscosity
l_e	m	Eddy characteristic dimension
τ_i	s	Eddy-droplet interaction time
τ_e	s	Eddy lifetime
g_i	kgm/s^2	External forces
h	m	Film thickness
α	[°]	Impingement angle
ν	m^2/s	Kinematic viscosity
La	-	Laplace number
$\overline{D}$	m	Number mean diameter
N	-	Number of secondary droplets
Oh	-	Ohnesorge number
r_m	-	Ratio of total splashing to incident mass
β	-	Ratio of lamella and impacting drop diameter
δ	-	Relative film thickness
τ_p	s	Relaxation time
Re	-	Reynolds number
r	m	Roughness
p	-	Secondary parcels
S	-	Source term
σ	kg/s^2	Surface Tension
T	K	Temperature
τ_t	s	Transit time
k	m^2/s^2	Turbulent kinetic energy
U	m/s	Velocity
x, y, z	m	Cartesian coordinates
We	-	Weber number

Subscripts

a	Advancing
lv	Between droplet (liquid) and vapor interface
cr	Critical value
d	Dynamic
0	Initial value (before impact)
$leid$	Leidenfrost
lf	Liquid film
max	Maximum
n	Normal
s	Secondary droplet (after impact)
t	Tangential
V	Volumetric
w	Wall

Acronyms

CHF	Critical Heat Flux
DPSF	Discrete Particle Separated Flow
QUICK	Quadratic upstream interpolation for convective kinetics
RANS	Reynolds-averaged Navier-Stokes equations
SPH	Smoothed Particle Hydrodynamic

Chapter 1

Introduction

The following thesis aims to accurately represent the interaction between an impinging spray and a solid surface through computational modeling. This is a complex and challenging relationship, which may be of interest for a great deal of industrial applications„ such as spray wall cooling process and spray injection in internal combustion engines.
This chapter will begin by enlightening the reader about the factual objectives of this paper, then will disclose the several reasons behind the choice of such theme, and finally will proceed to do an extensive literature review.

1.1 Objectives

The objective of this dissertation is to implement the model of spray-wall interaction presented by Ma et al. [41] in our in-house code. In order to do so, an extensive literature review is performed aiming to enrich the mathematical component of such model.
Our in-house spray-wall interaction code, was iniatilly developed according to the research of Kalantari [29], and was brung to fruition in Rodrigues [62]. During the development of this work, a great deal of attention was paid to the impinging and wall conditions, as well as to the droplet morphology. These terms represent the bigger opportunity to expand the applicable operation conditions of our spray-wall interaction model. Simulations were carried out for predicting the outcome of flows, including liquid film formation, droplet breakup, and spray evaporation. Consequently, this study will help to define and specify the properties of secondary droplets with great accuracy.

1.2 Motivation

The impact of liquid drops onto a solid surface has generated a great deal of interest from the scientific community ever since some of its applications have become clear and relevant to several other fields of research. The utter understanding of this phenomenon can lead to a series of scientific breakthroughs and subsequently to the optimization of different industrial applications such as spray cooling, coating, ink-jet printing, sprinklers systems or even internal combustion engines. As previously referred, another apropos application is concerned with studies about polluting gases resulting from any sort of spray impingement. In this scenery, internal combustion diesel engines play a dominant role in the fields of transportation of goods and passengers and also industrial applications. As mentioned in Khana et al. [32], one of the most important phenomenon in the umbilical relationship between air-fuel mixing and combustion is the droplet-wall interaction. Therefore, we must fully understand this process in order to reduce exhaust applications and adopt a more environmental-friendly approach. Taking into account everything previously mentioned, CFD codes can be considered a very valuable component of this analysis as they can replicate almost every test conditions. So, it is of great interest to a lot of fields of study to optimize the accuracy of such codes.

1.3 Overview

The present dissertation is organized with five chapters. The current chapter aimed to give a succinct view to the reader of the objective and motivation, as well as of the structure one will encounter as the reading continues.
In chapter two, a detailed literature review was performed. The study and analysis of the relevant background is fulcral for the comprehension of the work itself. This chapter is subdivided into three sections , which represent three different types of impacts: drop impact into wet surface, drop impact into non-heated and dry surfaces, and finally drop impact into heated and dry surfaces.
The third chapter contains the mathematical formulation and corresponding implementation of the spray-wall interaction model. At this stage, the continuous and dispersed phases are distinguished, as well as the boundary conditions used.
The results of the numerical analysis are presented and examined in chapter four. They are compared with the ones exhibited in Rodrigues [62]. Finally, the last chapter summarizes the most important conclusions obtained throughout this research and also presents some suggestions for future work.

Chapter 2

Literature Review

The following chapter aims to review some of the more important papers, according to our objectives, regarding spray-wall impingement. This chapter will be divided into three sections, following this order: impact onto wet wall in section 2.1 , followed by impact on heated and dry surfaces in 2.2, and finally impact on dry and non-heated surfaces in 2.3 .

2.1 Drop Impact onto Wet Wall

Droplet impact onto a wet wall, which implies the presence of a liquid film , illustrates a very important conceptual situation with several applications. For example, if on one hand it is advisable to avoid this layer in situations of diesel engines cold-starting , on the other it is recommended in cooling systems applications or even in spray painting production lines.

2.1.1 Transition Criteria

The presence or formation of a liquid film over the impingement surface is a very common phenomenon during the spray-wall process. This aforementioned film changes entirely the wall condition because it increases the energy dissipation rate of incident drops and, thereafter, the chance of splash. Hereupon, several researchers have come to the conclusion that one of the most substantial factors when analyzing this type of impact is the depth/thickness of the liquid film [77]. The size and number of splashed drops fluctuates plenty, depending upon the relative thickness of the surface film. In this sense, it has become very important to establish an as accurate as possible way to compute the value of the relative liquid film thickness present in each and every node of our grid. The film thickness can be found in literature described as:

$$\delta = \frac{h_{lf}}{D_0} \quad (2.1)$$

As we can see, it is the ratio between the film thickness and the initial diameter of the drop. Recalling one of the motivations of this work, many spray and coating applications, for instance, seek to minimize splashing, which can be manipulated by appropriate combinations of experimental parameters such as velocity and droplet size. Below, the displayed table elucidates on its effect on the volume of a variety of splashed products.

Table 2.1: Volume (μl) of the total splashed products at 3.15 m/s of a 2.0 mm droplet of the listed fluid onto a dry surface or a liquid film of the same fluid [77].

Fluid	Relative Film Thickness		
	0	0.1	10
Heptane	4.00	1.76	6.41
Hexadecane	0.43	1.38	8.91
DI water	0	1.29	1.22

It is , therefore, very clear that we need to include our relative thickness in the transition criteria , in order to obtain a trustworthy representation of the real phenomenon. Yarin and Weiss [81] explored the physical behavior of a single drop impingement on a wet surface and proposed a correlation for the splashing-deposition limit under thin film conditions ($\delta < 0.1$), establishing that the splash/non-splash criteria is clear at thin film impact and becomes insensitive to the variation of the film thickness at this range. A transition criteria *K* has been set to explore the splash/deposition limits [60]. The *K* parameter was introduced by Mundo et al. [47] and Yarin and Weiss [81] in 1995, and posteriorly Cossali et al. [18] found that K could indeed well characterize the splash/deposition limit. Above a critical value of *K*, splash is expected. The *K* parameter is an interesting alternative to Weber and a good candidate to generalize results taking into account effects of viscosity for low viscosity liquids. This parameter is a combination of Weber and Ohnesorge numbers, both particularly relevant in this study.

$$K = Oh^{-0.4} \times We \quad (2.2)$$

When setting the transition criteria, a distinction had to be made according to Ma et al.[41] regarding the type of liquid film present:

1. Shallow pool - It´s considered when $\delta < 1.2$;
2. Deep pool - It´s considered when $\delta > 1.2$.

In wet wall impact cases, the possiblities are :

Splash	K_3
Uncertain Region	K_2
Deposition	K_1
Rebound	

Table 2.2: Framework of droplet impingement

According to Pan and Law [53], rebounding and absorption are respectively favored for small and large *We*, being that absorption is facilitated for $\delta << 1$ and $\delta \approx 1$.

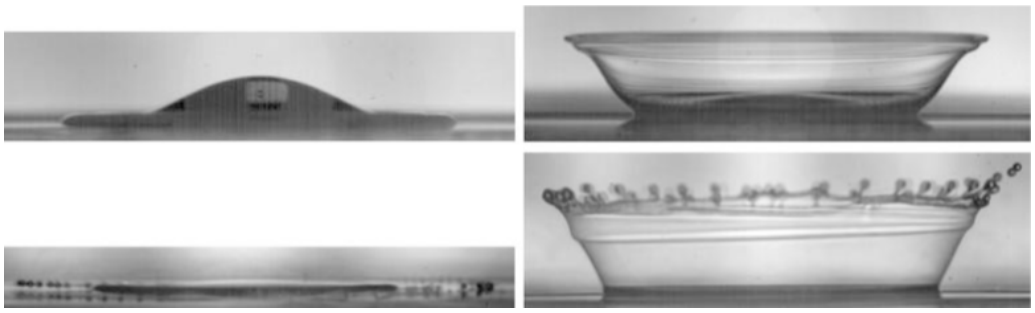

Figure 2.1: Outcomes of a drop impact on a wetted solid surface. Top left: deposition without formation of crown; top-right: formation of crown without break-up; bottom: splashes with (right) or without (left) formation of crown. [60]

Film thickness is not, although, the only parameter to influence the evolution of impingement. According to Vander Wal [77], when considering impact upon a dry surface, the action of viscosity (ν) promotes splashing by fostering a kinematic gradient in the advancing fluid front. Nevertheless , for impact on a thin fluid film ($\delta < 0.1$) the effect of drop fluid viscosity is opposite: the thin film interferes with the advancing fluid front to generate a kinematic gradient,

whereby a fluid with low viscosity and surface tension will experience the maximum acceleration difference and hence splash prior to fluids with higher ν. On the other hand, if the disparity in fluid viscosity has consequences in the splash or non-splash phenomenon, the role of the surface tension (σ) does not fluctuate a lot. This is, high surface tension retards droplet release from either a spreading droplet upon a dry surface or from a crown rim as produced during impingement upon a liquid film. In other words, high surface tension inhibits splashing, regardless of whether the receiving surface being either dry or a thin fluid film.
Based on the parameter *K* formula aforementioned, a lot of thresholds regarding the splash/non-splash interaction can be found in the literature. Cossali et al. [18] set this frontier as :

$$K_{cr} = 2100 + 5880\delta^{1.44} \quad \textbf{(2.3)}$$

More recently, after comparing their experimental results with Marengo and Tropea [43] correlations, Qiyu and Holden [28] established the splash frontier for thin film as:

$$(We \cdot Re)^{0.25} = 25 + 78^{1.44} \quad \textbf{(2.4)}$$

As seen, this transition criteria comes in terms of Oh and Re, as they found it to be more widely related to fluids of different viscosities. Also following this relation, Huang and Zhang [28] proposed that the coalescence/splashing threshold can be represented accurately by:

$$(We \cdot Re)^{0.25} = 25 + 7\delta^{1.44} \quad \textbf{(2.5)}$$

According to Okawa et al. [51], in the case of normal impact of single drops on a plane water surface, the *K* parameter is roughly constant at the deposition-splashing limit ($K \approx 2100$) , however, it varies according to the impingement angle (α). In our case, the impingement angle is constant.
Our in-house spray-wall interaction model was configured to follow Bai et al. [5] conditions, which are presented in table 2.3:

Table 2.3: Regime transition criteria

Wall Status	Regime transition criteria	Critical Weber number
Wetted	Stick->Spread	$We \approx 2$
	Rebound-> Spread	$We \approx 20$
	Spread -> Splash	$We \approx 1320La^{-0.183}$

As can be seen above, our existing critical parameter to separate regimes was initially based on Weber number.

2.1.2 Post-Impingement Features

The term ”splash” can be used to indicate the formation of secondary drops (droplets) after a primary impact, according to Cosssali et al. [18].
When a drop collides with a fluid interface, the fluid inside that very drop experiences a violent redirection from vertical to radial. According to Zou et al. [82], this collision may result in floating, bouncing, coalescence, or splashing (illustrated in figure 2.2), although not all of them are relevant to this dissertation. These possible outcomes depend on several factors mentioned above. For instance , a high impact velocity (which corresponds to a high Reynolds number) of

drop will puncture the air coating between the drop and the intended target resulting in a deep crater, and consequently in the formation of secondary droplets induced by capillary breakup.

Figure 2.2: Splash example with $We = 1392$ [22]

One of the most important parameters to influence the properties of the secondary droplets is the liquid film depth. Early on , Hobbs and Osheroff [27] reached the simplistic conclusion that the number of secondary droplets increases with decreasing film thickness. Later, researchers as Okawa et al.[51], empirically came to the conclusion that *N* is not dependent on δ in the case of drop impingement on a deep liquid, for instance.
Stanton and Rutland [74] deducted that the type of regime to be implemented had to do with the impact energy, that is, rebound stick and spread occurs at low *We* , whereby splashing occurs at high impact energy, and, consequently, high *We* number. Later, Senda et al. [68] also classified the drop-wall interaction process into high and low impact cases, setting the transition criteria at *We* $= 300$. In the lower energy regime, three types of disintegration mechanisms are detected based on the dimensionless film thickness, as mentioned in table 2.4:

Table 2.4: Low energy impact disintegration mechanisms. [68]

δ	<0.6	[0.6;1.35]	>1.35
Number of ejected particles	1	4	1

When the impact energy verified is above the threshold established and mentioned above, the total number of secondary droplets is expressed as:

$$N^s = r_m \frac{D_0^3}{D_s^3} \quad (2.6)$$

Bai and Gosman [5], established in 2002 a most-likely range of variation for r_m, once this ratio was believed to be affected by several parameters such as the droplet *We* and *La* , wall roughness

and pre-existing wall film thickness. These authors established the following relation for the number of secondary droplets per splash:

$$N_s = a_0 \left(\frac{We}{We_{cr}} - 1 \right) \quad (2.7)$$

where $a_0 = 5$. Okawa et al. [51] concluded, based on their experiments of a single water drop impact onto a plane water surface, that N_s is not dependent on δ in the case of drop impingement on a deep liquid, and so the proper relation is :

$$N_s = max \left[4.97 \times 10^{-6}; 7.84 \times 10^{-6} (\delta)^{-0.3} \right] K^{1.8} \quad (2.8)$$

In their studies, Kalantari and Tropea [30] divided their classification of secondary droplets properties in function of the impact angle. Their results indicated that in the case of normal impact conditions the secondary-to-incident mass (r_m) and number of secondary droplets increase linearly with the impact *We* based on the normal component of the impact velocity (We_n), whereby in the case of oblique impact condition the secondary-to-incident mass and number of secondary droplets behave quite differently: these two variables decrease with the impact *We* based on the normal component of the impact velocity and increase with the impact Weber number ratio $\frac{We_t}{We_n}$.

Table 2.5: Equations for some post-impingement characteristics according to Kalantari ao Tropea [30]

	Normal impact	Oblique impact
N_s	$N_s = (2.16 \times 10^{-3} We_{0n} + 8.96 \times 10^{-2}) N_0$	$N_s = (7.1 We_{0n}^{-1.14}) N_0$
r_s	$r_{m_n} = 6.74 \times 10^{-3} We_{0n} - 0.204$	$r_{m_{ob}} = 35 We_{0n}^{-1.63}$

In that same paper, Kalantari and Tropea [30] also concluded that the normal component of velocity after the impact does not correlate well with the normal velocity component of the impinging droplet, while the tangential component of the ejected droplets correlates closely with the impingement tangential velocity. Also following this brand of thinking, Okawa et al. [51] proposed the following correlations for the secondary-to-incident mass ratio to normal and oblique impacts, respectively:

$$r_{m_n} = 1.56 \times 10^{-3} exp^{4.86 \times 10^{-4}} \quad (2.9)$$

$$r_{m_{ob}} = r_{m_n} exp^{0.115(\alpha - 10)} \quad (2.10)$$

In what concerns the diameter of secondary droplets , Kalantari and Tropea [30] described that the average secondary droplet size D_s increases slightly with increasing impact droplet size. They established the following relation :

$$D_s = -0.003 We_n + 1.2 \quad (2.11)$$

Before them, Senda et al. [68] had already proposed a relation between the diameter of im-

pinging and secondary droplets as:

$$\frac{D_s}{D_0} = 3.932 \times 10^2 K_{mod}^{-1.416} \quad (2.12)$$

where $K_{mod} = WeOh^{0,4}$.

2.2 Drop Impact onto Non-heated and Dry Surfaces

Drop impacts on dry surfaces exhibit more complicated flow patterns than those on the wetted surfaces, due to the influence of the surface texture, which includes wettability and roughness. Most applications of drop impingement involve relatively high temperatures, while a few concern maintaining relative low wall temperatures. Some examples include fuel drop impingement in internal-combustion engines with direct fuel injection or spray cooling in fire extinguishing and electronics cooling systems.
In the following section, the focus will be set on the determination of the boundaries between impingement regimes and the post-clash features of secondary droplets.

2.2.1 Transition Criteria

Rioboo et al. [58], following his experimental work, presented the possibility of six different outcomes from this type of collisions:

1. Deposition – the drop is only deformed and stays on the surface during the entire process;
2. Prompt splash – droplets are ejected directly from the region between the surface and the liquid in the spreading phase of the lamella;
3. Corona splash – a crown is formed during the spreading phase and eventually breaks up into droplets;
4. Receding break-up – droplets are left on the surface during the receding phase of the impact;
5. Rebound – the entire drop rebounds from the surface;
6. Partial rebound – part of the drop stays attached to the surface while other part rebounds.

This classification was at the time more detailed than the ones already present in the literature, which consisted basically in four outcomes: stick, rebound, spread and splash. This states can be related to each other through the Weber number, increasing in the precise aforementioned order. In their experiments, Rioboo et al. [58] observed some particularities like the fact that prompt splash occurs when the impacted surface has a elevated level of roughness, or for example that the key factor that distinguishes the occurrence of rebound or partial rebound is the dynamic receding contact angle. This latter distinction is not recognized by most of the investigators , which lump these two regimes together. For this reason, and also because the pre-existing code was constructed this definition, the term ”rebound” is used herein to indicate whether there is a complete or partial detachment of the liquid from the wall after initial contact.
When analyzing these types of spray-wall interactions, one must take into account the elevated number of parameters that affect the outcome of such interaction. These parameters range

from liquid properties, size, velocity and impact angle of the impinging drop to the topography of the target surface.

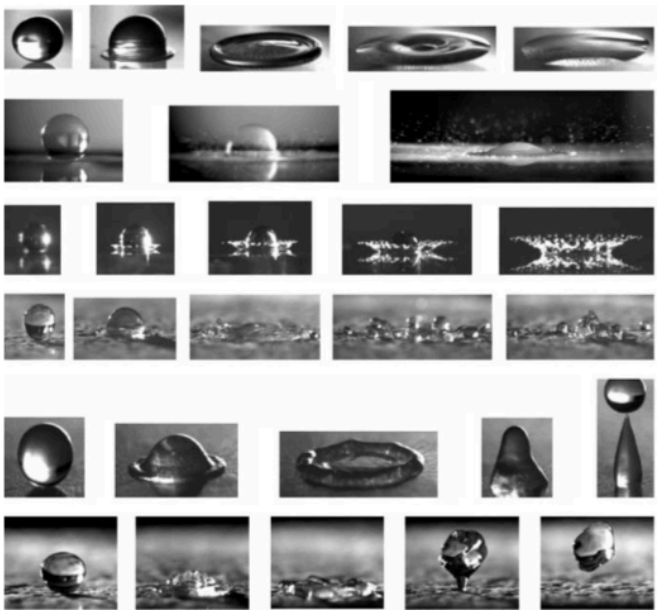

Figure 2.3: Outcomes of a drop impact on a solid dry surface. From top to bottom: Deposition, prompt splash, corona splash, receding break-up, partial rebound, complete rebound. [58]

For instance, according to Kalantari and Tropea [31], increasing the surface roughness will yields in increasing the size of secondary spray, as well as the total secondary-to-incident mass ratio, although , the influence of the surface roughness on this mass ratio becomes weaker if the ratio of $\frac{We_t}{We_n}$ increases (which translates to oblique impact condition). There are a lot of different transition criteria present in the literature, but in general all of them include dimensionless parameters such as the aforementioned Weber, Ohnesorge, Laplace and Reynolds numbers. In the model presented by Mundo et al. [46] the transition criteria used are based on a dimensionless variable *K*, which was set as :

$$K = OhRe^{1.25} \quad (2.13)$$

where *K* is a function of the Reynolds and Ohnesorge numbers. To demarcate the frontier between splash and deposition, they set this parameter as $K = 57.7$, which means that if *K* features a smaller value there will be deposition, otherwise splash is expected. These experiments showed that roughness influenced the outcome of splashing, while the transition condition for deposit or splash remained unchanged with increasing wall roughness. Authors like Lee and Ryou [37] , later, were in agreement with Mundo et al. [46] regarding the deposition and splash frontier, being that in both cases the splash criteria were appropriate at low *Re* region but relatively underestimated at high *Re* region, which makes the drop easier to splash at dry wall impact cases.
In their studies, Vander wal et al. [78] concluded that only the power-law correlation based on the *Oh* and *Re* numbers proved fruitful in defining a clear boundary between splash and non-splash regimes, and established it as :

$$Oh \times Re^{0.6089} = 0.8458 \quad (2.14)$$

where the Reynolds parameter is contained in the range of : $0 < Re < 7500$. Notably, Vander

Wal et al. [78] concluded that the splash/non-splash boundary has an opposite dependence upon each parameter, this is, high surface tension acts to restrict splashing as fluid extension increases surface area and hence energy. Conversely, high viscosity acts to promote splashing. More recently, Palacios et al. [52] introduced the notion that although in impacts onto smooth surfaces the lifting of liquid usually implies the formation of secondary droplets, that may not hold for sufficiently low Reynolds numbers. In their work, they assumed splashing to be characterized not only by the lifting of some liquid from the solid surface, but also by the ejection of secondary droplets. They proposed the following splash/lifted liquid film threshold:

$$We_{splash} = 5.80Re^{0.5} + 4.01 \times 10^{7}Re^{-1.97} \quad (2.15)$$

The validity of this expression probably cannot be extended to Re numbers below 400. This expression means that under this value it is expected that a liquid film layer be lifted without the formation of secondary droplets, which will occur if such value is exceeded. For the threshold that separates deposition from clearly distinguishable splash outcomes, Palacios et al. [52] formulated the following:

$$We_{splash} = 4.43Re^{0.53} \quad (2.16)$$

where $Re <\approx 1000$.

Figure 2.4: Example of impact with splash. Adapted from Kittel et al. [34]

2.2.2 Post-Impingement Features

As aforementioned in 2.1, when a droplet impacts onto a solid surface, its kinetic energy is redirected into the radial direction by droplet spreading that stops at the maximum extent. Subsequently, the droplet retracts back under the action of capillary force, and it eventually sticks to or rebounds from the surface, depending on the impact conditions. According to Rioboo et al. [59], the deposition scenario consists of two stages: the kinematic and the actual deposition. In the kinematic stage, the radius of the drop base is autonomous of the physical properties of the liquid and the surface, whereby, in both cases, at the end, the drops spread over the surface and stay there. The ratio of the final lamella diameter related to the drop one (maximum spreading ratio) was set by Pasandideh-Fard et al. [24] as:

$$\beta_{max} = \sqrt{\frac{We + 12}{3(1 + \theta_a) + 4(\frac{We}{\sqrt{Re}})}} \quad (2.17)$$

where θ_a = dynamic advancing contact angle. Some years later, Ukiwe et al. [76] studied a series of models regarding the maximum spreading ratio, and came to the conclusion that the one proposed by Pasandideh-Fard et al. [24] agreed the most with their experimental data.

Starting from this assumption, Ukiwe et al. [76] considered that it was possible to obtain better agreement if they carefully considered the surface energy term at the maximum spread. Hereupon, they used the Young equation to obtain the surface energy at the maximum spread in terms of θ_y :

$$E_s = \pi\sigma_{lv}D_{max}h + \frac{\pi}{4}\sigma_{lv}D_{max}^2(1-\cos\theta_y) \quad (2.18)$$

where σ_{lv} and θ_y represent surface tension between the droplet (liquid) and the vapour interface, and Young contact angle, respectively. Combining the equations for the different energy terms and using the viscous term of Pasandideh-Fard et al. [24] they obtained an updated expression for the maximum spreading ratio:

$$(We+12)\beta_{max} = 8 + \beta_{max}^3\left[3(1-\cos\theta_y) + 4\frac{We}{\sqrt{Re}}\right] \quad (2.19)$$

More recently, Eggers et al. [23] made the distinction between high and low viscosity regimes, or better, one where viscosity may be neglected so that surface tension selects R_{max}, and other where viscous dissipation dominates surface tension, and the maximal radius R_{max} appears as a balance between inertia and viscosity. The connection between these two regimes depended on the interaction between viscous and capillary effects, so that the dependence on Re and We could be gathered into a single scaling relation. Hereupon, in the viscous regime, most of the initial kinetic energy is lost to viscous dissipation, resulting :

$$\beta_{max} = C \times Re^{1/5} \quad (2.20)$$

where $C = 1,113$. On the other hand, when viscosity can be neglected, the maximum radius is determined by a balance between inertia and surface tension. The result is:

$$\beta_{max} = (\frac{We}{6})^{1/2} \quad (2.21)$$

According to Wildeman et al. [79], for impact velocities and negligible surface friction at the solid surface (which they denominated "free slip"), approximately one-half of the initial kinetic energy is transformed into surface energy, independent of the impact parameters and the detailed energy loss mechanism. To complete, for impacts on a no-slip surface, also dissipation in the shear boundary layer at the solid surface is important. In this case, the spreading on a no-slip surface approaches that on a free-slip surface when the droplet viscosity is sent to zero. Wildeman et al. [79] concluded that good agreement was found between their models and experiments, both for impacts on lubricated surfaces (e.g. Leidenfrost droplet impacts) and for impacts on no-slip surfaces. They arrived to the following expressions for free-slip and no-slip surfaces, respectively:

$$\beta_{max} = \sqrt{\frac{4}{1-\cos\theta}\left(\frac{1}{24}We+1\right)} \quad (2.22)$$

$$\frac{3(1-\cos\theta)}{We}\beta_{max}^2 + \frac{\alpha}{\sqrt{Re}}\beta_{max}^2\sqrt{\beta_{max}-1} = \frac{12}{We} + \frac{1}{2} \quad (2.23)$$

where $\alpha = 0.7$.
If the impact energy and consequently the We number are high, we should expect splash. From

here forward, the properties of splash droplets will be presented. For the estimation of the size of the secondary droplets, Bai et al. [5] proposed a chi-squared distribution function as follows:

$$f\left(D_s\right) = \frac{1}{\overline{D}} exp\left(-\frac{D}{\overline{D}}\right) \quad (2.24)$$

where $\overline{D}$ represented the number mean diameter and was expressed by :

$$\overline{D} = \frac{D_0}{6^{1/3}} \left(\frac{r_m}{N_S}\right)^{1/3} \quad (2.25)$$

Lee and Ryou [37], on the other hand, opted to determine the secondary droplet size of ejected droplets through the mass conservation law. They arrived to the following expression :

$$D_s = \left(\frac{r_m}{N_s}\right)^{1/3} D_0 \quad (2.26)$$

Continuing this quotation, Lee and Ryou [37] took advantage of the experimental data obtained by Naber and Farrel [49], and established that the number of ejected droplets can be determined as follows:

$$N_s = 0.187We - 4.45 \quad (2.27)$$

Bai et al. [4] proposed the following after a carefully review of the Stow and Stainer [75] work:

$$N_s = a_0 \left(\frac{We}{We_{cr}} - 1\right) \quad (2.28)$$

Applications such as fuel injection are demanding, since not only is the mass distribution between the deposited film and the secondary spray important, but also the size and velocity distribution of the secondary spray. According to Roisman et al. [64], the velocity of the secondary spray of low viscosity liquids can be successfully estimated using the inviscid solution, based on the analysis of propagation of the kinematic discontinuity and the ejection of the liquid sheet. However, the energy lost due to viscosity can influence the magnitude of the absolute velocity of the sheet and thus of the secondary droplets.

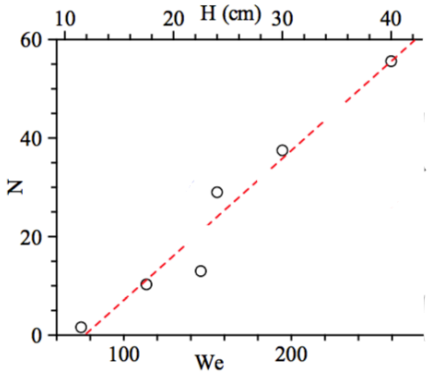

Figure 2.5: The dependencies of the number of emitted droplets as functions of the impact height and the Weber number for water drop impacting. Adapted from Chiang et al. (2017).

In order to calculate the velocity of the droplets, the energy conservation law is often utilized. As in the spreading phase, the kinetic and surface energy of the incident drop should

balance the kinetic and surface energy of splashing droplets and the dissipative loss due to the action of viscosity. The splash kinetic energy is the unknown quantity (from which the velocity parameter will be calculated), whereas the remaining terms are easily determined with the exception of the energy dissipation parameter for which attention must be directed towards. Lee and Ryou [37] determined the total velocity of droplets after impingement by using their own derived relationship for the dissipated energy instead of the critical Weber number:

$$E_D = \frac{K_v C_w We_{0N} \beta_s^4}{r_m Re_{0N}} - \frac{12 C_w}{r_m} \quad (2.29)$$

where $K_v = 4.5$ and $C_w = (\frac{r_m}{N_s})^{1/3}$.
During this literature review, it became clear that there is still a lot of dissonance regarding both the transition criteria and the post impingement features according to different researchers. A clear example of this discord is the literature regarding the effect of viscosity: If on one hand Vander Wal et al. [78] concluded from his experiments that high viscosity promotes splashing, Rahmati and Zarareh [56] recently considered that by increasing the Reynolds number, the effect of viscosity decreases and consequently the splashing mechanism becomes stronger, as illustrated in figure 2.6.

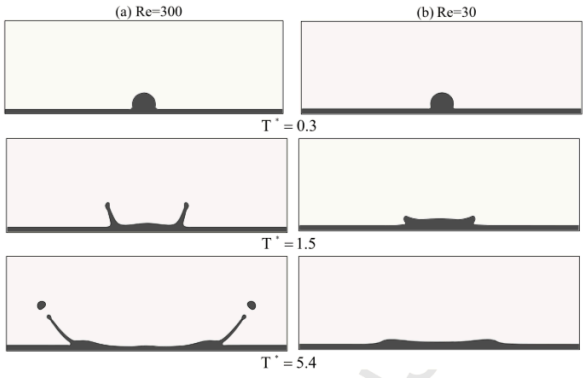

Figure 2.6: Influence of Reynolds number, and consequently of viscosity in splash promotion. Adapted from Rahmati and Zarareh et al. [56]

2.3 Drop Impact onto Heated and Dry Surfaces

The interaction between a spray and a hot surface can be observed in an extensive panel of applications nowadays, such as spray cooling or in internal combustion engines. As previously mentioned, for an isothermal drop impact onto a dry solid surface, the outcome depends mainly on the impact velocity, drop diameter, and of substrate morphology and wettability. Nevertheless, when the temperature is altered and becomes higher, the phenomenon of drop impact can change significantly and different thermodynamic phenomena can be observed, namely film evaporation, nucleate boiling, transition boiling, atomisation and film boiling.
In this section, the concept of ”Leidenfrost temperature” will be extensively exploited due to his importance in the new model, as well as all the thermodynamic phenomena supra-cited and the correspondent transition criteria. There will be a review upon the factors influencing the post-impingement features of secondary droplets.

2.3.1 Transition Criteria & Thermodynamic Phenomena

Heat transfer in drop impingement on a heated wall is strongly influenced by magnitude of wall temperature relative to the liquid's saturation temperature. When T_w is smaller than T_{sat} , heat transfer is dominated by heat conduction from the wall to the liquid, and evaporation due to mass transfer along the liquid-gas interface. Briefly, when T_w begins to exceed T_{sat}, the drop boils on the heated wall, and small bubbles form inside the drop. On the other hand, at even higher wall temperatures, when T_w exceeds the Leidenfrost temperature (T_{leid}), a thin vapor layer instantly forms between the drop and the wall, which greatly decreases liquid-solid contact and culminates in substantial deterioration of heat removal from the wall.
Generally, from a heat transfer perspective we can find that there are four different evaporation regimes to be identified: film evaporation, nucleate boiling, transition boiling, and film boiling. All are identified in figure 2.7 . At first, Bernardin et al. [7] pointed out that wall temperature (T_w) and the impact Weber number are the two most important parameters governing impact behavior and heat transfer, whereby a couple of months later Bernardin et al. [8] also incorporated the influence of surface roughness in their studies. For instance, in their studies they concluded that for impinging drops protruding features on rough surfaces promotes the rupture of the liquid film resulting from the impact, which reduced the pressure beneath the droplet and consequently yielded a lower (T_{leid} when compared to a "polished" surface.

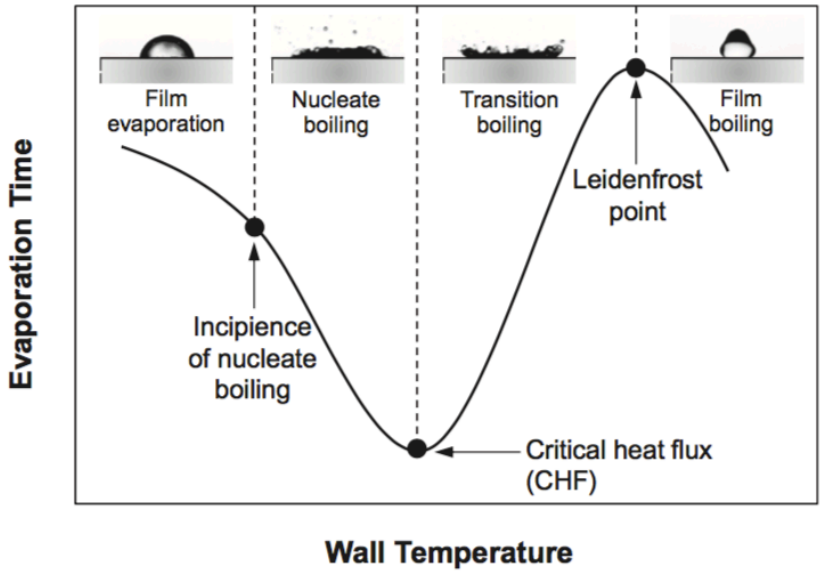

Figure 2.7: Heat transfer regimes associated with a drop impinging a hot wall. Liand and Mudawar [40]

In the region presented in figure 2.7 as "film evaporation" , the temperature registers below the saturation temperature (T_{sat}) of the liquid and no bubbles form, whereby the main heat transfer mechanism is natural convection. The following regime, denominated "nucleate boiling", occurs when the surface temperature exceeds the aforementioned T_{sat} and does not reach the critical heat flux point (CHF). Moita et al. [44] reported that a single bubble or circular bubble rings are formed in the drop immediately after impact in this regime, which was attributed to entrapped air between the liquid-solid frontier. Chen et al. [15] described it as "so violent nucleate bubble generation" that the vapor bubbles burst abruptly on the free

surface of the droplet, resulting in explosive ejection of tiny droplets.
Continuing the analysis, the next regime spans the region between the CHF and Leidenfrost points, and is denominated as "transition boiling". In this zone, according to Nikolopoulos et al. [50] the splashing of the liquid associated with the formation of a ring detached from the spreading lamella is predicted, while the remaining film becomes highly disturbed and breaks into a large array of droplets. Moreover, formation of vapor bubbles within the bulk of the liquid was predicted.
For the final regime, Leidenfrost temperature is of the utmost importance. T_{leid} can be identified as the lowest wall temperature of the film boiling regime. In general, two different methods have been encountered in the literature to determine T_{leid} : thermodynamic and hydrodynamic. According to Liang and Mudawar [40], the thermodynamic method defines T_{leid} as the wall temperature at which total evaporation time of the drop is longest, while the hydrodynamic one depends on temperature measurements to determine when a stable vapor layer begins to form between the drop and the wall. For instance, due to the poor thermal conductivity of vapor layer, the heat transfer is significantly reduced. Thus, efforts to avoid the Leidenfrost effect are of great importance for improving spray cooling heat transfer.
The Leidenfrost phenomena can be divided according to the impact type, this is, between sessile and impinging drops. Taking into account this classification, the Leidenfrost point associated with sessile drops it is called *static*, and the one associated with impinging drops it is refered to as *dynamic*, whereby the latter carries more relevance to this study.
For an impinging drop, the liquid contact with the wall is mainly the result of drop momentum (unlike for a sessile drop, which is only gravity) which increases the Leidenfrost temperature. For that reason, Rein [57] introduced the concept of a dynamic Leidenfrost temperature , T_{leid_d} , being that :

$$T_{leid_d} > T_{leid} \quad (2.30)$$

Furthermore, he added that the dynamic Leidenfrost temperature would be a function of the Weber number.
Earlier this year, Chen et al. [15] updated and defined T_{leid_d} as the minimum temperature of the surface at which the impacting droplet rebounds without splashing. So, and recovering the previous interrupted analysis, the final regime is referred to in literature as "film boiling" , and occurs when the surface temperature is very high above the Leidenfrost point. When the surface temperature registers such high values, the number of activated nucleation site and the bubble generation rate increase rapidly. Herewith, the vapor layer formation is facilitated. So, in this regime, a vapor layer forms immediately after impact , making it impossible for the droplet to make further contact with the surface. As aforementioned, the poor conductivity of the vapor layer leads to no boiling behavior being observed. Thus, the droplet is supported by its own vapor and bounce off the surface without ejecting tiny droplets.
Regarding the transition criteria, Rein et al. [57] presented the scheme illustrated in 2.8: As can be deduced from 2.8 , at high *We* drops would always splash, and if the wall temperature is smaller than the saturation temperature, this splash happens above a critical *We*. The process of breakup could be enhanced by boiling initiated by contacts formed between the liquid and the wall, therefore, it was to be expected that splashing begins at *We* numbers smaller than the critical Weber number obtained in the case of cold walls, as those dashed lines indicate. The drops would rebound completely without disintegration whenever $T_w > T_{leid_d}$, however, as long as the wall temperature is not too high the rebound is connected with the formation of many

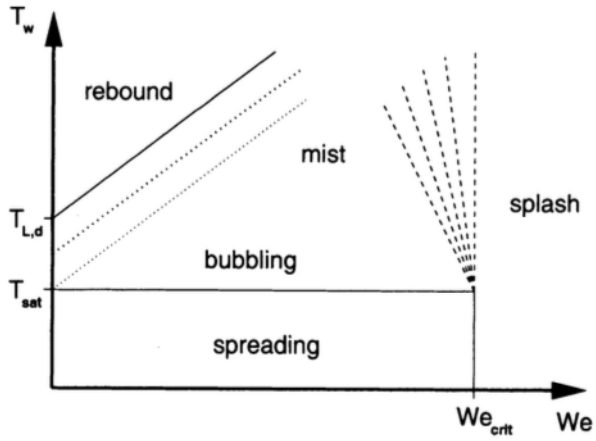

Figure 2.8: Different outcomes of drop interactions with hot surfaces in dependence on the surface temperature and the Weber number.T_{L_d} equals T_{leid_d}. Adapted from Rein [57]

secondary droplets that are ejected away from the rebounding drop, resembling a mist. The transitional regime between disintegration including mist formation and rebound is indicated by dotted lines.

More recently, Bertola [11], based on his study on impact morphology of millimetric water drops on a polished aluminium surface with surface temperatures varying between 50 and 400 °C , was able to identify five main impact regimes: secondary atomisation, breakup/splashing, rebound, rebound with secondary atomisation, and breakup with secondary atomisation. They are represented in figure 2.9.

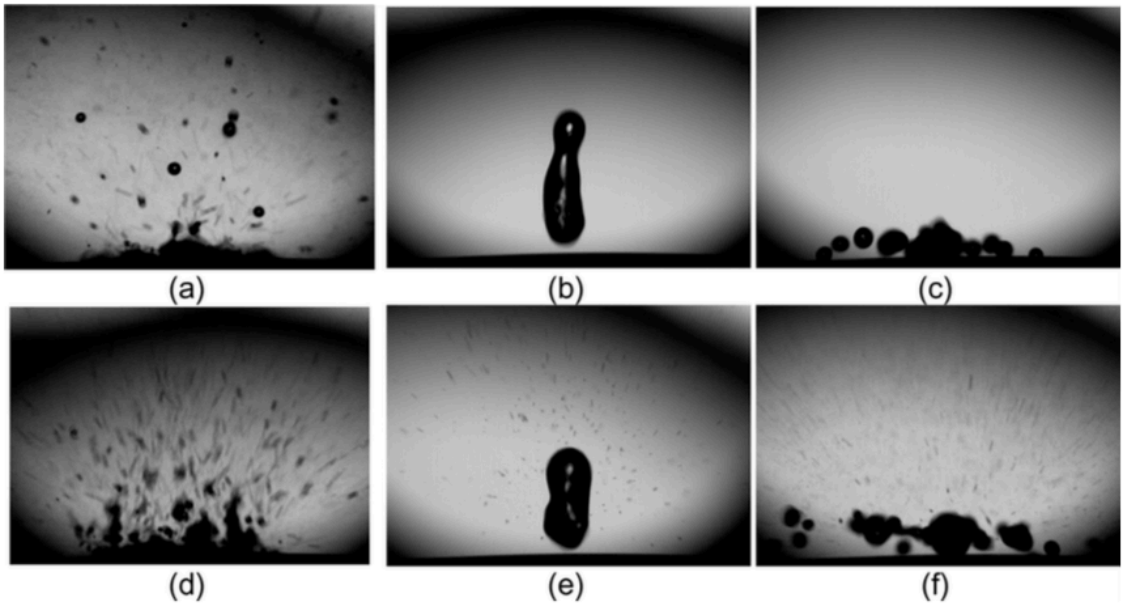

Figure 2.9: Impact regimes according to Bertola [11]: secondary atomisation (a, d), rebound, (b), splashing (c), rebound with secondary atomisation (e), splashing with secondary atomisation (f).

In his study, he concluded that for high temperatures ($T_w > 350C$), two outcomes were possible: drop rebound for low Weber numbers, and drop breakup/splashing for higher Weber numbers. Bertola [11] explains that rebound occurs because at high temperatures a vapour film forms between the liquid and the surface immediately upon impact, as aforementioned,

which acts as a lubricant layer, reducing energy dissipation during drop spreading and recoil. This translates that, at the end of recoil, there would still be some kinetic energy available for rebound. He went on and added that, if at the end of the expansion stage, there was still an excess of the initial impact kinetic energy that was not converted into surface energy or dissipated, the drop would break into smaller droplets (splashing). These two regimes would both fit in the film boiling region. For smaller temperature, they observed two additional regimes: rebound with secondary atomisation and splashing with secondary atomisation. On both cases, Bertola [11] reported an unstable vapour film between the drop and the impact surface, which allowed local contact between the liquid and the hot surface, where vapour bubbles could grow and generate secondary atomisation. These two regimes can be associated with the transition boiling region.
As aforementioned, the transition between the rebound and rebound with secondary atomisation regimes defines T_{leid_d} , and this is subsequently defined, generally, with the following form:

$$T_{leid_d} = A + BWe^n \quad (2.31)$$

where *A*, *B* and *n* are constants that assume different values for different authors. Yao et al. [80] established them, respectively, for small drops as T_{sat}, 135.6 and 0.09. On the other hand, Bertola and Sefiane [10] proposed that for bigger drops $(D > 4mm)$: *A*=164.72 , *B*=29.97 and *n*=0.38. Altough, none of this values fitted Bertola [11] transition from dry to secondary atomisation rebound observed in his work, which he concluded suggests the transition is very sensitive to several parameters such as the drop diameter and the relative velocity between the drop and the surface. Using the Leidenfrost Point Model proposed by Bernardin et al. [9] , Bertola [11] arrived to the following expression:

$$T_{leid_d} = 162 + 7.3We^{0.32} \quad (2.32)$$

Bertola [11] also proposed the following correlation for the critical value of the *K* parameter, above which splash/drop desintegration is expected :

$$K_{cr} = 649 + 3.76(\frac{r_w}{D_0})^{-0.63} \quad (2.33)$$

where r_w is the surface roughness. Years before, Castanet et al.[13] identified three main regimes and proposed the following transition criteria:
In their experiments of water droplets impacting onto a smooth heated plate made of nickel, Castanet et al. [13] were able to construct the diagram using a correlation beetween the *K* parameter and the dimensionless surface temperature T^*, which is as follows:

$$T^* = \frac{T_s - T_{sat}}{T_{leid} - T_{sat}} \quad (2.34)$$

When analyzing drop impingement onto heated surfaces, one must also consider the hydrodynamic perspective, this is, the hydrodynamic behavior associated with the impact. Boiling of an impacting droplet on a heated surface occurs when the surface temperature is sufficiently high to nucleate vapor bubbles at the solid-liquid interface, which is a flagrant part of various technical applications such as fuel injection in combustion engines. For instance, Khavari et al. [33] divided boiling behavior into four regimes: spreading regime, bubbly boiling regime (which in some literature represents the fusion of aforementioned nucleate and transition boiling) ,

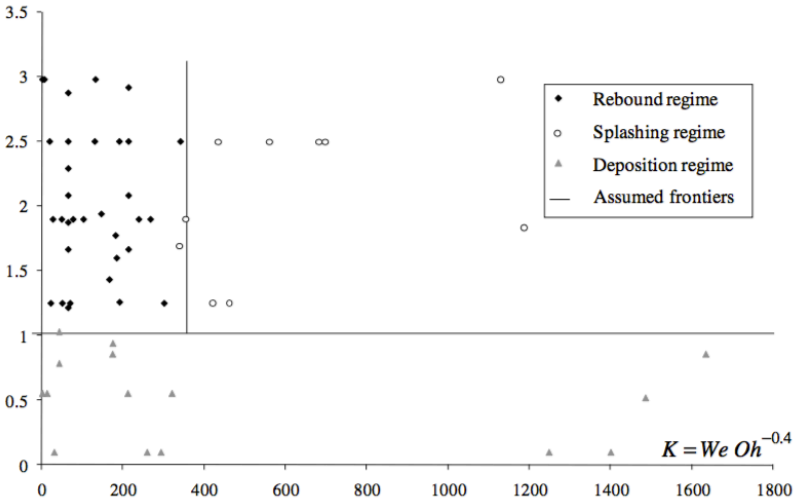

Figure 2.10: Castanet et al. [13] mapping of the different impact regimes.

fingering boiling regime and Leidenfrost regime. Staat et al. [73] measured the wetted area during drop boiling using interferometric high-speed imaging, and identified four different regimes: deposition, contact-splash, bounce, and film-splash. They also identified two transition lines, one towards splashing, corresponding to increasing *We*, and another towards Leidenfrost state for increasing T_w:

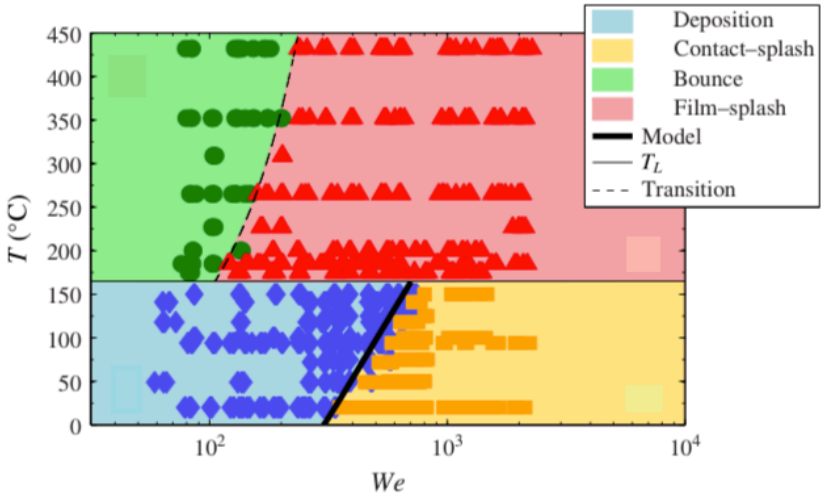

Figure 2.11: Transition lines towards splashing and Leidenfrost regime. Adapted from Staat et al. [73].

2.3.2 Post-Impingement Features

Contrary to the impact on non-heated surfaces, heat transfer between the liquid drop and the hot surface alters the dynamics involved during impact, and consequently the properties of secondary droplets. For an isothermal drop impact without phase change, the outcome is determined mostly by the impact parameters, liquid properties and substrate morphology, whereby on the impact onto a hot surface all these factors are accompanied by nucleate boiling, film boiling, phase change phenomena and other thermodynamic effects. Nevertheless, some authors have brought forward, more recently, some research regarding this subject. Despite the

difficulty to recognize clearly the limits of the heat transfer regime transition boiling , Akhtar et al. [3] proposed the following expression for the maximum spreading diameter:

$$\frac{D_{max}}{D_0} = 0.003We + 3.21 \quad (2.35)$$

Breitenbach et al. [12], used an arithmetic mean value of the velocity magnitude to show the distribution of the velocity magnitude of secondary drops during thermal atomisation. They concluded that the measured high velocity droplets arise only during the first instants of drop impact. The velocity decreases greatly at later times, according to both theoretical and empirical observations. 2.12.

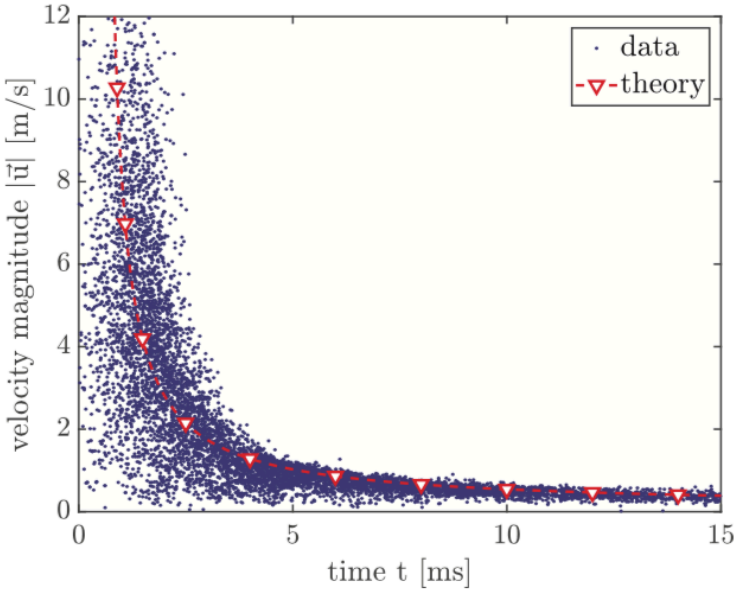

Figure 2.12: Velocity magnitude of the measured droplets as a function of time in comparison with the theoretical model. Breitenbach et al. [12]

Using a dual-mode phase Doppler system to measure the velocity and size of the secondary droplets for various impact parameters and surface temperatures, Breitenbach et al.[12] arrived to the following expression for the theoretical velocity of the secondary droplets:

$$u_d(t) \approx K \frac{e_w(T_{w_0} - T_{sat})}{\sqrt{\rho_v \sqrt{\rho_l}} L \sqrt{\pi} \sqrt{t - \tau(t)}} \quad (2.36)$$

where *L* is the latent heat of evaporation, e_w is the thermal effusivity of the solid material, *K* is an adjustable coefficient obtained by fitting the experimental data (usually around the unity). The coefficient $\tau(t)$ can be represented by $\Delta z_0/u_d$, where Δz_0 accounts for the axial position of the measurement volume above the impact surface and the resulting time delay in the data acquisition.

Regarding the number of ejected droplets, Hamdan et al. [26] in their experimental studies of droplet behaviors impacting on a hot surface above the Leidenfrost temperature and on a inclined surface, were able to extract the following expression from the their experimental data:

$$N = We_n^{0.8} exp\left(\frac{-78}{We_n}\right) \quad (2.37)$$

In the film boiling regime, Akhtar and Yule [3]obtained the following correlation for the number of secondary droplets:

$$N = 0.0427We + 10.46 \quad (2.38)$$

It can be pointed that according to the early work of Cossali et al. [19] an increase in liquid viscosity considerably increases the size of secondary droplets in the film boiling regime, but has no significant effect in nucleate boiling one. Also, increasing impact velocity in this regime increases lamella spread, which subsequently decreases the size of secondary droplets.

2.4 Summary

This chapter was divided into impact onto wet wall in section 2.1 , followed by impact on heated and dry surfaces in 2.2, and finally impact on dry and non-heated surfaces in 2.3, once these are the most important phenomena tested in our spray/wall interaction model.
During this literature review, it became clear that parameters such as wall temperature and condition (wet/dry), along with the incident drops properties, are critical to the outcome of such impingement. Going forward, we'll see the inclusion of these parameters in the general context of our *in-house* model.

Chapter 3

Mathematical Model

This chapter describes the mathematical model used to predict the consequences of droplets impinging onto a solid surface.
The majority of jet engines employ some sort of internal combustion, in order to directly heat the air. Such process usually involves multiphase flows during the combustion process, particularly during the injection of the fuel spray into the combustion chamber: The spray is referred to as the dispersed phase and is surrounded by a fluid (the continuous phase) all over the entire domain of simulation. In the following sections, these two phases will be exposed in detail, as well as the measures used to account for the interaction between them, and the boundary conditions employed in the model.

3.1 Continuous Phase

The name of this section comes from the fact that the fluid is regarded as continuum. Once the focus of this CFD investigation is not at the level of microscopic length, but rather at a macroscopic one, it is perfectly acceptable to ignore molecular structure of matter and molecular motions. Therefore, macroscopic properties as density, pressure, temperature, and velocity are considered to be well-defined at infinitely small points, and are assumed to vary continuously from one point to another. The conservation laws of physics state that the mass of a fluid is conserved, and the rate of change of momentum equals the sum of the forces on a fluid particle, being that the governing equations for the gas phase represent the mathematical statements of such laws. The resulting time-averaged partial differential equations are the continuity and momentum equations, which in index notation and for a steady, incompressible, viscous, Newtonian fluid are expressed as:

$$\begin{aligned} \rho\frac{\partial\overline{U_i}}{\partial x_i} &= S_m \\ \rho\frac{\partial\overline{U_i}}{\partial x_j}\overline{U_j} &= -\frac{\partial\overline{P}}{\partial x_i} + \frac{\partial}{\partial x_j}(\mu\frac{\partial\overline{U_i}}{\partial x_j} - \rho\overline{u_i^{'}u_j^{'}}) + S_{U_i} \end{aligned} \tag{3.1}$$

where $u_i^{'}u_j^{'}$ represent additional turbulent stresses (Reynolds stresses) and the overline represent time-averaged quantities. In its turn, S_m and S_{U_i} are source terms used to account for the interactions between the fluid and any suspended particulate material. These two equation comprise the Reynolds-averaged Navier-Stokes equations, or RANS. The partial differential equations for a steady incompressible flow can be reduced to a single convective-diffusive conservation equation by introducing a general variable property per unit mass ϕ :

$$\frac{\partial(\rho\phi U_i)}{\partial x_i} = \frac{\partial}{\partial x_i}\left[\Gamma_\rho\frac{\partial\phi}{\partial x_i}\right] + S_\phi \tag{3.2}$$

In equation 3.2, Γ is the effective diffusion coefficient for quantity ϕ, and S_ϕ is is the general source term. This equation is divided the following way : the convective term is on the left

side, whereas the diffusive and source terms are on the right side. Equation 3.2 is referred to in the literature as transport equation for property ϕ. The module of turbulence applied in this code is the $k-\varepsilon$ presented by Launder and Spalding [35], which is widely and thoroughly tested. Equations 3.1 connect with the Boussinesq hypothesis, also presented by Launder and Spalding [35], and and from that connection results the Reynolds stresses related to the mean rates of deformation :

$$\rho\overline{u_i'u_j'} = -\mu_t\left(\frac{\partial\overline{U_i}}{\partial x_j} + \frac{\overline{U_j}}{\partial x_i}\right) + \frac{2}{3}\rho k\delta_{ij} \quad (3.3)$$

where $k = \frac{1}{2}(\overline{u_i'^2} + \overline{v_i'^2} + \overline{w_i'^2})$ represents the turbulent kinetic energy per unit mass. Also,δ_{ij} is the Kronecker delta and , finally, μ_t is the turbulent dynamic viscosity, which is space and time dependent property, and consequently of the local turbulent characteristics of the flow. μ relates to the k and ε in fully developed, isotropic turbulence through dimensional analysis with the following expression:

$$\mu_t = C_\mu\rho\frac{k^2}{\varepsilon} \quad (3.4)$$

where C_μ is a dimensionless model constant.
Recovering equation 3.2, and by replacing the property ϕ with the corresponding variable, we're able to get the special forms of the partial differential equations for the continuity, momentum, enthalpy, vapour mass fraction, turbulent kinetic energy, or dissipation. This is presented in table3.1. The source term presented in equation 3.2 is divided in two components:

$$S_\phi = S_{\phi,d} + S_{\phi,g} \quad (3.5)$$

where $S_{\phi,d}$ specifies the source term of the droplet, and $S_{\phi,g}$ the one of the gas.

Table 3.1: Substitution coefficients for ϕ. Adapted from Rodrigues et al. [63]

ϕ	$S_{\phi,g}$	$S_{\phi,d}$	Γ
U_i	$-\frac{\partial}{\partial X_i}(P+\frac{2}{3}k) - \frac{\partial}{\partial X_j}\frac{2}{3}\mu_t\frac{\partial\overline{U_j}}{\partial X_i} + \rho g_i$	$\overline{S_{U_i,d}}$	$\mu+\mu_T$
T	0	$\overline{S_{T,d}}$	$\frac{\mu}{Pr} + \frac{\mu_T}{Pr_T}$
Y_d	0	$\overline{S_{Y_i,d}}$	$\frac{\mu}{Sc} + \frac{\mu_T}{Sc_T}$
K	$G-\rho\varepsilon$	$\overline{S_{k,d}}$	$\mu + \frac{\mu_T}{\sigma_k}$
ε	$C_1\frac{\varepsilon}{k}G - C_2\rho\varepsilon$	$\overline{S_{\varepsilon,d}}$	$\mu + \frac{\mu_T}{\sigma_\varepsilon}$

The variable G presented in table 3.1 refers to the usual turbulence energy production term, and is defined as:

$$G = \mu_t\left[\frac{\partial\overline{U_i}}{\partial x_j} + \frac{\overline{U_j}}{\partial x_i}\right]\frac{\partial\overline{U_i}}{\partial x_j} \quad (3.6)$$

The value for each of the various dimensionless constants used is given in table 3.2 , and are the ones suggested by Launder and Spalding originally, based on the analysis of numerous turbulent free jets and mixing layer simulations.

Table 3.2: Coefficients from the turbulence model $k-\varepsilon$. Adapted from Launder and Spalding [35].

$C_{\varepsilon 1}$	$C_{\varepsilon 2}$	$C_{\varepsilon 3}$	σ_k	σ_ε	P_{r_t}	S_{c_t}	P_r	S_c
1.44	1.92	1.1	1	1.3	0.6	0.85	$\frac{\mu C_p}{k_G}$	$\frac{\mu}{\rho C_d}$

According to Launder and Morse [36], these values can be assumed to provide model accuracy in the range from about 10% to 50%, depending on the flow.
In order to obtain the solution for the governing equations, a finite- difference method was used to obtain a system of algebraic equations that can be solved numerically. This process involves the integration of the transport equation 3.2 using a control-volume-based technique, whereby the quadratic upstream interpolation for convective kinetics (otherwise known as QUICK) scheme of Leonard [38] has been adopted for this purpose. This scheme is free from artificial diffusion and gives more accurate solutions with grid spacing much larger than that required by other schemes. This scheme minimizes numerical diffusion errors by involving more neighboring nodes: two upstream and one downstream nodal values. The face value (ϕ) is then obtained from a quadratic function passing through two bracketing nodes and a node on the upstream side. Figure 3.1 shows the face of a control volume surrounding a central node with a value ϕ_P. For this face, using a uniform grid for simplicity, the value of ϕ is expressed by:

$$\phi_w = \frac{1}{2}\left(\phi_P + \phi_W\right) - \frac{1}{8}\left(\phi_P - 2\phi_W + \phi_{WW}\right) \quad (3.7)$$

This equation verifies if the convective velocity component U_W is assumed to have the direction shown in figure 3.1. The first term in equation 3.7 is the central difference formula, and the second is the important stabilizing upstream-weighted normal curvature contribution.

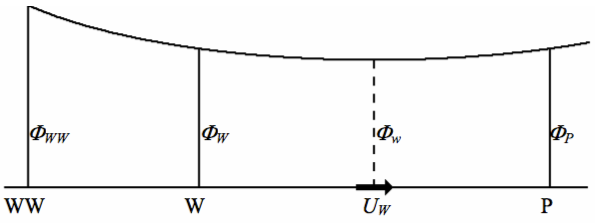

Figure 3.1: Nodal configuration for a control volume face.

Some of the variables are not stored at the nodes of an ordinary control volume, namely the scalar quantities like pressure or temperature. In fact, if velocities and pressures were to be defined at the nodal points, a highly non-uniform pressure field could act like a uniform field in the discretized momentum equations. Therefore, a staggered grid for the velocity components is used so they are defined at the (scalar) cell faces in between adjacent nodes.
This time, considering a three-dimensional approach to this problem, a hexadron-shaped cell containing node *P* has now six neighboring nodes.
The terminology employed in figure 3.2 depicts a geographical approach with *N*, *S*, *W* and *E* representing north, south, west and east face of node *P*. *T* and *B* stand for top and bottom face.
The general form of the discretized equations for any dimensional problem stands as:

$$A_P^\phi \phi_P = \sum A_i^\phi \phi_i + S_U^\phi \quad (3.8)$$

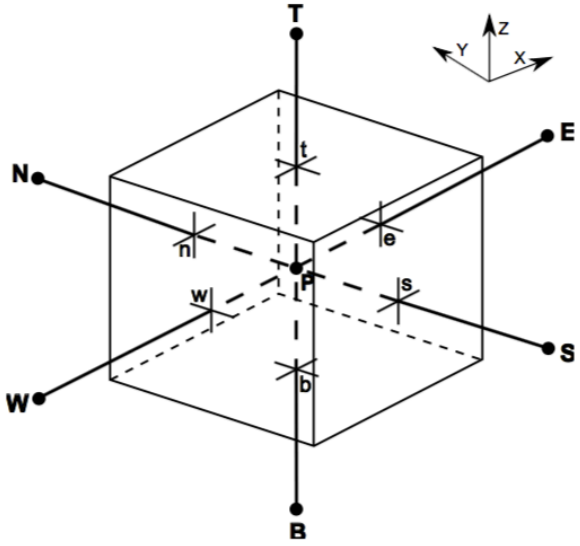

Figure 3.2: Nodal configuration for a control volume. Adapted from Rodrigues [62].

where A_i are the the neighbouring coefficients (A_W, A_E, A_S, A_N, A_T, A_B) and ϕ_i are the values of the property ϕ at the neighboring nodes. Also, A_P^ϕ is the coefficient at node *P* and is represented by:

$$A_P^\phi = \sum A_i^\phi + (F_i - F_{i-1}) - S_P^\phi \quad (3.9)$$

where, subsequently, *F* is the convective mass flux per unit area. Combining equations 3.8 and 3.9 we get:

$$\sum A_i^\phi(\phi_P - \phi_i) + (F_i - F_{i-1})\phi_P = S_U + S_P^\phi\phi_P \quad (3.10)$$

where $(S_U + S_P^\phi\phi_P)$ is the linearized source term. The work of Barata [6] is important because it prevents that the resolution of the set of equations for the complete field could lead to negative values of A_i^ϕ, by subtracting $A_i^\phi\phi_P$ from both sides of equation 3.8 and therefore eliminating the negative contribution of A_i^ϕ and simultaneously enhancing the diagonal dominance of the coefficient matrix. This way, in the CFD code already present, the diagonal dominance of the coefficient matrix is ensured and enhanced by rearranging the difference equation for the cells in which the coefficients A_i^ϕ become negative.
Based on the semi-implicit method for pressure-linked equations (SIMPLE) algorithm [55], the solution procedure for the continuous phase is achieved.

3.2 Dispersed Phase

In this section, the method used to solve the gas phase, which is based on the solution of the equations for energy, momentum and mass will be presented.
The governing equations for the gas phase represent the mathematical statements of the conservation laws of physics. Such laws state that the mass of a fluid is conserved, and the rate of change of momentum equals the sum of the forces on a fluid particle. In the present work the

dispersed phase was treated using the Lagrangian reference frame, therefore it will be discussed in more detail in this section. Hereupon, a combination of Lagrangian and Eulerian framework is more adequate in this multiphase flow. Therefore, although the dispersed phase equations come in the Lagrangian form in order to be able to move with each element, the fluid phase are still expressed in the Eulerian way, as this approach is very popular when particle loading is high.

Regarding turbulent dispersion, it is based on the concept of energy containing eddies, and their trajectories can be obtained by solving the particle momentum equation through the Eulerian fluid velocity field. Throughout the turbulent flow field, there are interactions between particles and the local turbulent eddies, which are constituted by a instantaneous property consisting of a mean quantity (obtained directly from the Reynolds averaged equations) and a fluctuating quantity (obtained from a Gaussian distribution with a standard deviation proportional to the locally predicted value of $\sqrt{k}$). The key point in this stochastic treatment is to determine the length of time over which these random components exist, namely the interaction time of the particle and the turbulent eddy. This stochastic model includes a experimental probability density function (PDF), from which the initial droplet size distribution of the spray is selected. The basic idea behind this is to track a single PDF for droplet position, where this PDF would represent a group of droplets having the same physical properties and initial conditions, due to the number of drops in the real scenario being usually very large.

As long as all the forces acting on a droplet immersed in a turbulent flow are mathematically quantified, the droplet trajectory can be determined by solving its equation of motion. This equation can be deduced from Newton's Second Law of Motion. For two-phase flows, in order to obtain the trajectory of a particle in a fluid flow, we can assume three details:

1. The particle is assumed to be spherical;

2. Particle-particle collision is neglected;

3. The particle density is assumed to be much larger than the surrounding fluid density.

When a drop is in motion, it experiences different forces known as Basset, virtual mass, and Magnus forces: the Basset force results from the transitory nature of the droplet's boundary layer , the virtual mass force originates because of the difference in acceleration between the fluid and the droplet, and the Magnus force results when a rotating droplet is subjected to a non-rotating fluid. This three enumerated assumptions, when valid, neglect several of this forces previously in action. The assumption 1 is perfectly acceptable due the static pressure gradient being small and the drag in these particles being similar from that on a sphere. Due to absence of crossflow in this simulation, the air flow rate is never high enough to induce drop deformation, and consequently this assumption is always applicable. The second assumption 2 is also plausible once, for instance, most Lagrangian models known as discrete particle separated flow (DPSF) neglect droplet-droplet interactions and the volume occupied by the droplets [70]. For assumption number three 3, it is perfectly plausible to admit that most of the densities of impinging drops are larger (in some cases much larger even) than that of water. Taking into account these aforementioned assumptions, the drop momentum equation becomes immensely simplified:

$$\frac{\partial U_i}{\partial t} = \frac{1}{\tau_p}(U_{G_i} - U_i) + g_i \quad (3.11)$$

where τ_p is the droplet relaxation time, and g_i is the external forces (i.e. gravity, centrifugal and Coriolis forces). This relaxation time is defined as the rate of response of droplet acceleration to the relative velocity between the droplet and the carrier fluid, and the correspondent mathematical expression is :

$$\tau_p = \frac{24\rho D^2}{18\mu C_D Re_p} \quad (3.12)$$

where Re_p is particle Reynolds number, given by:

$$Re_p = \frac{\rho \left| U - U_G \right| D}{\mu} \quad (3.13)$$

and the drag coefficient can be obtained through [21]:

$$C_D = \begin{cases} \left(\frac{24}{Re_p}\right)\left(1 + 0.15 Re_p^{0.687}\right) & Re_p < 1000 \\ 0.44 & Re_p \geq 1000 \end{cases} \quad (3.14)$$

Hereupon, replacing equations 3.13 and 3.14, a new expression is obtained for the droplet relaxation time:

$$\tau_p = \frac{m}{3\pi\mu D} \frac{1}{1 + 0.15 Re_p^{0.687}} \quad (3.15)$$

So, recovering equation 3.11, one can verify that it is a first-order, non-homogeneous, nonlinear differential equation. The droplet momentum equation can be analytically solved over small time steps Δt, in which the instantaneous fluid velocity and the drop relaxation time are assumed to be constant. Therefore, by knowing the new droplet velocity at the end of each time step, a droplet trajectory can be built:

$$\begin{cases} U_i^{new} = U_{g_i} + (U_i^{old} - U_{g_i}) e^{-\Delta t/\tau_p} + g_i \tau_p (1 - e^{-\Delta t/\tau_p}) \\ x_i^{new} = x_i^{old} + \frac{\Delta t}{2}(U_i^{new} + U_i^{old}) \end{cases} \quad (3.16)$$

Applying equations 3.16 to each of the components of the Cartesian coordinates system considered provides three dimensional trajectory of the particles.
With that said, determination of the instantaneous fluid velocity and the evaluation of the time (Δt) of interaction of a droplet with a particular eddy is crucial. The time step is the eddy-droplet interaction time, characterized by τ_i and meaning the lower value between the eddy lifetime (τ_e) and the eddy transit time (τ_t). Each eddy is characterized by a length scale (l_e), a time scale (τ_e), and a velocity (fluctuating). The eddy size and the eddy lifetime can be estimated from the local turbulence properties (k and ε) along the droplet trajectory:

$$\begin{gathered} l_e = B\frac{k^{3/2}}{\varepsilon} \approx C_\mu^{3/4}\frac{k^{3/2}}{\varepsilon} \\ \tau_e = A\frac{k}{\varepsilon} \approx 0.2\frac{k}{\varepsilon} \end{gathered} \quad (3.17)$$

where A and B are two dependent constants extracted from experimental data present in [69]. The eddy transit time, τ_t , is the minimum time a particle would take to cross an eddy with characteristic dimension,l_e, and is given by:

$$\tau_t = -\tau_p \ln\left(1 - \frac{l_e}{\tau_p \left| U_{G_i} - U_i \right|}\right) \quad (3.18)$$

Equation 3.18 has no solution when $l_e > \tau_p |U_{G_i} - U_i|$, which in the practical sense translates to when the linearized stopping distance of the particle is smaller than the eddy size. When this occurs, it's assumed that the particle is trapped by the eddy and the interaction time is the eddy lifetime.
Knowing the interaction time and randomly sampled fluctuating fluid velocity, it is possible to solve equation 3.16 for the droplet trajectory. The eddy-droplet interaction time corresponds to the time step; at the end of each time step, a new fluctuating fluid velocity is sampled from a new PDF, which is generated using the local turbulence properties. After this, the local properties of the new droplet location are used to determine the new interaction time.
This isotropic model has been extended in the present work to account for cross-correlations or anisotropy. So, to obtain the fluctuating velocities $u^{'}$ and $v^{'}$ at every time step, two randomly sampled fluctuating velocities u_1' and v_2' are used as well as a correlation coefficient R_{uv} :

$$\begin{cases} u_f^{'} = u_1^{'} \\ v_f^{'} = R_{uv} u_1^{'} + \sqrt{1 - R_{uv}^2} u_2^{'} \\ R_{uv} = \frac{\overline{u_f^{'} v_f^{'}}}{\sqrt{\overline{u_f^{'2}} \overline{v_f^{'2}}}} \end{cases} \quad (3.19)$$

where R_{uv} fluctuates from 0 to 1.

3.3 Model Implementation

There are innumerable ways to computationally implement the aforementioned model, presented in Rodrigues et al. [63]. The already in place, and also used, CFD code follows the numerical procedure beneath :

1. The initial conditions are established by defining both the staggered grid and the characteristics of the initial drops;
2. A converged solution of the gas flow field is calculated disregarding the source terms of the dispersed phase;
3. The discrete parcels are traced through the flow field in the dispersed phase and the values of the source terms are calculated;
4. The gas flow is recalculated considering now the source terms of the dispersed phase;
5. Steps 2 and 3 are repeated until convergence is reached;
6. Post-processing of the data occurs.

This procedure is illustrated in figure 3.4. Obviously, in dilute flows each of the phases presented earlier in sections 3.1 and 3.2 are influenced by each other motion via displacement of mass as well as momentum and energy transfer effects. This interaction is then portrayed by treating particles as sources of mass, momentum and energy in the gaseous phase, whereby a two-way coupling method is favored. Beneath, table 3.20 with the source terms due to the particles is presented. It's worth mentioning that this source terms are calculated for each Eulerian cell of the continuous phase and can be divided into two parts:

$$S_{\phi,p} = S_{\phi,i} + S_{\phi,m} \quad (3.20)$$

where $S_{\phi,i}$ represents the source term due to inter-phase transport , and $S_{\phi,m}$ specifies the transfer caused by evaporation.

Table 3.3: Source terms of the dispersed phase. Picked from Sommerfeld [72].

$S_{\phi,p}$	$S_{\phi,i}$	$S_{\phi,m}$
$\overline{S_{\rho,p}}$	0	$\sum \frac{\dot{m}_k N_k}{U_{i,j}}$
$\overline{S_{U,p}}$	$-\sum \frac{\dot{m}_k N_k}{U_{i,j}} \left[(U_k^{t+\Delta t} - U_k^t) g_i \Delta t\right]$	$\sum \frac{\dot{m}_k N_k U_{ia}}{U_{i,j}}$
$\overline{S_{T,p}}$	$-\sum \frac{N_k}{U_{i,j}} (L\dot{m}_k + Q_L)$	$\sum \frac{\dot{m_k} N_k}{U_{i,j}} C_{vap}(T_k) T_k$
$\overline{S_{Y_{air},p}}$	0	0
$\overline{S_{Y_{water},p}}$	0	$\sum \frac{\dot{m}_k N_k}{U_{i,j}}$
$\overline{S_{k,p}}$	$\overline{U_j S_{U_j i}} - \overline{U_j S_{U_j i}}$	$\overline{U_j S_{U_j m}} - \overline{U_j S_{U_j i}} + \frac{1}{26}\overline{U_j U_j S_m} - \frac{1}{2}\overline{U_j U_j S_m}$
$\overline{S_{\varepsilon,p}}$	$C_{\varepsilon 3} \frac{\varepsilon}{k} \overline{S_{ki}}$	$C_{\varepsilon 3} \frac{\varepsilon}{k} \overline{S_{km}}$

3.4 Initial Conditions

The conditions in which this computational simulation occurs are presented in Panão et al. [54], a study aiming at replicating the conditions found in homogeneous charge combustion ignition (HCCI) engines. The simulated tunnel, presented in figure 3.5, consists of a cross section of $150 \times 50mm^2$ with $270mm$ of depth. There is a longitudinal symmetry plane which originates a cross section of $75 \times 50mm^2$, and allows to decrease the computational power necessary. The injector is located in the middle of the tunnel, $Z_{in} = 135mm$.
The measurements were made using a two-zone system, as illustrated in figure 3.3. The first zone covers the radius of $0 - 3mm$ directly below the injector, and the second of $3 - 6mm$ downstream.

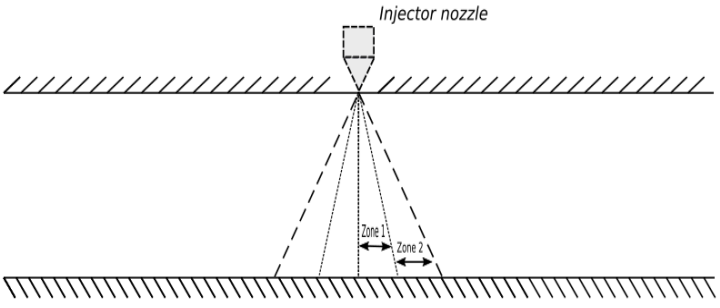

Figure 3.3: Measurement areas.

The solution domain is constituted by six boundaries:

1. an inlet plane - the transported variables are specified on the boundary with uniform profiles;

2. an outlet plane - normal gradients for all dependent variables are set to zero ($\partial\phi/\partial n = 0$);
3. a symmetry plane $-$ $\partial\phi/\partial n = 0$, except for the velocity component normal to the boundary, which is zero;
4. three non-slip walls $-$ velocity components relative to the wall are zero. The wall function method, described in detail by Launder and Spalding [35], is used to prescribe the boundary conditions for the velocity and turbulence quantities, assuming that the turbulence is in state of local equilibrium.

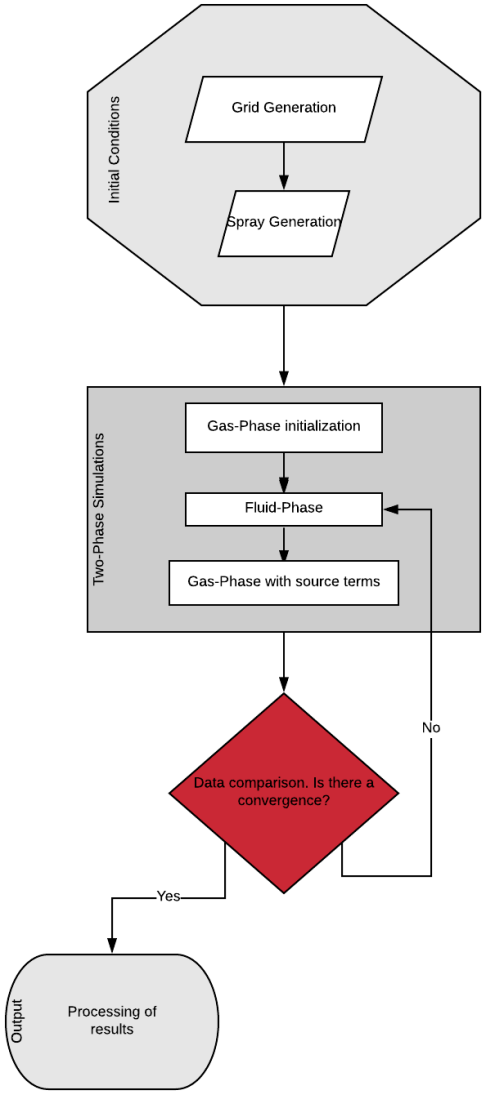

Figure 3.4: Flowchart of the computational process.

As aforementioned , the already in place model suffered a series of changes. The backbone of this reform consists in the work of Ma et al. [41]. This chapter also contains sections which address the atomisation process and the transition criteria implemented, as well as an introduction of the Leidenfrost effect taking into account the research of Cheng [16]. Also extremely important are the properties of secondary droplets, which are addressed in this chapter, as

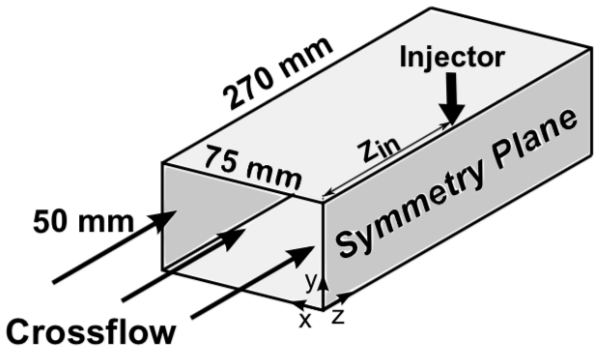

Figure 3.5: Configuration of simulated tunnel. Adapted from Rodrigues et al. [63].

well. These were included in the splash sub-model modifications. Finally, a description of the changes made to increase the accuracy of the impact point is presented.

3.5 Atomisation Process

In this dissertation, the spray is assumed to consist of a collection of isolated incident drops. This is key when simulating properly the spray impact process, because there is a need to ensure that the initial characteristics of the incident drops are estimated with adequate accuracy. Thus, the input data required for invoking such methodology comprises both size and velocity of the liquid particles at some point relative to the impact surface.
Relatively to the atomisation process, and to the gathering of such informations (size and velocity) , the model in place is the one used on Bai and Gosman [5]. A variable consisting of *N* parcels is chosen to be large enough that the whole spray is represented statistically. To achieve such goal, the spray is represented in circular cross-sections, in this case, two of them. Each

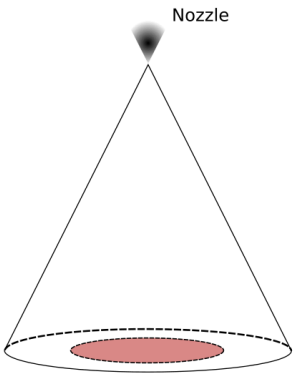

Figure 3.6: Two measurement zones.

section is penetrated by an equal number of parcels. The size of the drops in each parcel (D_k) are sampled from the PDF's provided in the measurements according to the following equation:

$$D_k = D_{min} + \gamma_1(D_{max} - D_{min}) \quad (3.21)$$

whereas the radial position in the measurement plane is:

$$r_k = r_{i-1} + \gamma_2(r_i - r_{i-1}) \quad (3.22)$$

γ_1 $\gamma 2$ are uniformly distributed random number between $[0; 1]$. D_{min} and D_{max} are selected from experimental work.
To determine initial drop velocity, the approach is based on an iterative procedure in which the axial velocity profiles of the free spray at the downstream horizontal plane are approximated as best as possible by mathematical expressions that are a function of the incident angle (θ). So, considering all the information previously mentioned, to determine the normal component of the velocity, one commences with a guessed value and makes repeated corrections until close agreement is obtained with the measured drop size-velocity correlations. In a complementary manner, the radial component of the velocity is obtained by reference to the normal velocity profile and by assuming a random circumferential angle (eta) with a value between $0°$ and $360°$ degrees. This process ends up creating a spray with a specific velocity magnitude by combining experimental data and a uniform circular ring of particles at the injector exit.

3.6 Impingement Regimes & Transition Criteria

The impact regimes present in this CFD model are all expressed in the model introduced by Ma et al. [41]. The representative scheme is presented in figure 3.7 As the scheme indicates, when

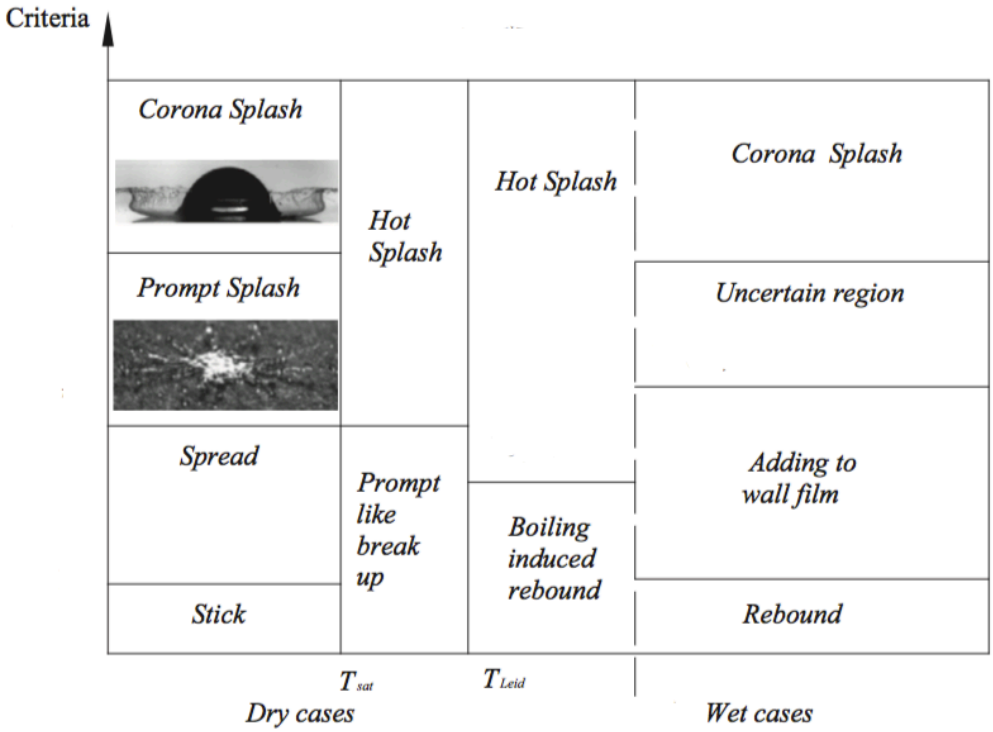

Figure 3.7: Framework of drop impingement used. Adapted from Ma et al. [41].

we're presented with an impact in dry wall, the temperature has a great deal of importance regarding the outcome. Depending on wall temperature, different outcomes are to be expected. If our saturation temperature has not been reached yet, we can expect stick and spread regimes (grouped in our *in-house* code as "deposition"), as well as prompt and corona splash. On the other hand, if our wall temperature exceeds the saturation point, but is shy of the Leidenfrost temperature, we'll have prompt like break-up, as well as hot splash (treated as corona splash). Finally, when our wall temperature exceeds the Leidenfrost point, rebound and hot splash are

expected.
When the wall records a liquid film layer, the temperature has significant less impact. In this case, the four impact stages defined by Ma et al. [41] are rebound, deposition, corona splash, and ”uncertain region”. In the latter, whether a drop splashes or not is determined by a random number between 0 and 1, because Ma et al. [41] found out that there are roughly equal splashed drops and non-splashed drops in such region.

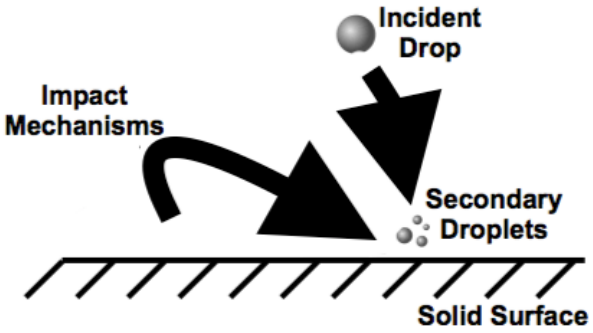

Figure 3.8: Schematic diagram of drop impacts onto a solid surface. Adapted from Rodrigues [62].

When approaching the prediction of the different impact regimes , one must consider all the mathematical details coming from different impingement conditions. With this said, the regime referred in the CFD model as ”Deposition” is a combination of stick and spread cases, whereby, whenever one of this occurs it is assumed that there is formation of secondary droplets being the wall wet at the impingement location. Therefore, this condition will affect the subsequent impact events. Moving on to the rebound regime, the mass of incident drop remains constant before and after wall impact, but the incident energy is more or less dissipated with droplet deformation. Rebound is verified both in dry and wet wall impact. This rebound model assumes that , as Bai and Gosman [4] proposed, the rebounding droplets have a negligible rotation effect.
Finally, the splash regimes takes place usually when the incident drops collide against the solid surface with high impact energy. This type of impact produces secondary atomisation and is by far the most complex to represent , mathematically speaking. In dry wall cases, the deposition/splash criterion of low temperature region (below the boiling point) is defined considering the incident energy and surface energy of droplets , presented in Bai and Gosman [5]. The rebound/splash criterion of high temperature region (above the boiling point and below the Leidenfrost temperature) was selected from Chen et al. [14], as well as the one for the super-high temperature region (above the Leidenfrost temperature). In wet wall cases, the criterion set for the rebound/deposition was selected from Cossali et al. [18]. All the transition criteria are displayed in table 3.4 . It’s worth referring that the wall film thickness is considered in some impact regimes, for instance, the rebound/deposition in wet wall cases is divided in shallow film impact ($\delta \leqslant 1.2$) and deep pool impact ($\delta > 1.2$). In this model, the criteria used for wet wall regime changes was the *K* parameter , whereby for the dry wall ones the criteria used was expressed in *We* numbers. Similarly to the stick and spread grouping, this model also had united corona and prompt splash, treating both as simply ”Splash”. Yet, an effort was made to separate the two during the dry impact case, due to the fact that secondary droplets present different characteristics for each case.

Table 3.4: Transition criteria applied in this model.

Wall Status	Wall Temperature	Transition Type	Transition criteria
Dry	$< T_{sat}$	Deposition/ Prompt Splash	$We = 289$
		Prompt Splash/Corona Splash	$Oh = 0.00446$
	$T_{sat} < T < T_{leid}$	Rebound/Splash	$We = 20$
	$> T_{leid}$	Rebound/Splash	$We = 14$
Wet	$< T_{sat}$	Rebound/Deposition	$\begin{cases} K = 12 & ,\delta \leqslant 1.2 \\ K = 15 & ,\delta > 1.2 \end{cases}$
		Deposition/Uncertain Region	$K = 1400$
		Uncertain Region/Splash	$K = 1400 + 9100\delta^{1,2}$

Regarding the rebound/splash transition on dry surfaces for temperatures above the saturation and below the Leidenfrost one , Chen et al.[14] presented a study in which they tested a diesel drop impinging on a hot surface and found out the diesel drop disintegrated when $We > 14$. On the other hand and more recently, Liang et al. [39] while studying drop impacts near the Leidenfrost point also witnessed this phenomenon. They concluded that by increasing We boiling transits from simple rebound or explosive detachment to explosive rebound gradually. Hence, the terminology used in 3.7 "Prompt like break up" is used to define this rebounding area. The Leidenfrost temperature formula used was proposed by Chen et al.[16]. In their studies, the conclusion was achieved that the dynamic Leidenfrost temperature (the one used in this particular type of impact) is highly dependent on the Weber and Ohnesorge number. In their experimental data, and through least squares fitting, the empirical correlation follows as:

$$T_{leid_d} = (13We^{0.5} + 22)Oh^{-0.2} + 48 \quad \textbf{(3.23)}$$

3.7 Properties of Secondary Droplets

In this section of this thesis, the methods used to predict quantitatively the properties of secondary droplets will be laid out. Properties such as velocity, diameter, size distribution or even trajectory are of extreme importance in order to comprehend and improve all sort of applications in which drop impingement is present.
Since the computational cost of tracking each and every secondary droplet would be too high, this model calculates only a statistical sample of the full population. This solution follows the Bai and Gosman model [5] where it is assumed that each incident droplet parcel can produces up to six secondary parcels (p). Each of these parcels contains an equal proportion of mass.
The total number of secondary droplets produced (N_s) follows the proposal of Bai and Gosman [5]:

$$N_s = a_0(\frac{We}{We_{cr} - 1}) \quad \textbf{(3.24)}$$

where a_0 is a constant with value of 5. The number of droplets per parcel can be defined as:

$$N_{s,p_a} D_{p_a}^3 = \frac{r_m D_0^3}{p_a} \quad (3.25)$$

In this model, the droplet splashing mass fraction was defined based on smoothed particle hydrodynamic (SPH) method and found it as a function of incident We and Re , as proposed by Ma et al. [42]. For a wet wall, Ma et al. [42] proposed the following relation:

$$r_m = \lambda 0.065(We - 40)^{0.6}(\delta + 0.074)^{-0.6}\left[1 - \exp(-0.018\frac{Re}{We}\tau)\right] \quad (3.26)$$

where λ is a correction factor respecting the difference between the actual secondary droplet fraction and the theoretical splashing fraction, and displays the value of 0,3. Also, τ represents the non-dimensional time and is defined as:

$$\tau = \frac{Ut}{D} \quad (3.27)$$

where U is the incident velocity.
When it comes to the dry wall impingement case, the non-dimensional film depth is considered to be zero so that the function is refitted as:

$$r_m = \lambda 0.041(We - 40)^{0.55}(0.074)^{-0.6}\left[1 - \exp(-1.328\frac{Re}{We}\tau)\right] \quad (3.28)$$

The distribution of splash angle is quite different between corona splash and prompt splash. For the corona case, the splash angle is usually very high due to the fact of this type of splash being associated with high energy impacts. Therefore, the ejection angle is set randomly between 30 and $90°$. Meanwhile, the secondary drops of prompt splash always fly along the wall, which means the splash angle is quite small ($0 < \alpha_s \leq 30°$).
When referring to secondary droplets size, our implemented model follows the correlation proposed by Roismann et al. [65] for wet walls:

$$D_s = \begin{cases} 24DRe_0^{-1/2} & Re_0 > 500 \\ D(0.65 + 0.017\exp\left[\frac{Re_0 - 252}{73.5}\right]) & Re_0 < 500 \end{cases} \quad (3.29)$$

The velocity of secondary droplets (U_s) is assumed to be a combination of two components : normal and tangential components of the velocity.

$$U_s = U_{s_T} + U_{s_N} \quad (3.30)$$

The tangential component can be described as:

$$U_{s_T} = U_{0_T} C_f \quad (3.31)$$

from where one can deduce that the tangential component of secondary droplets velocity is proportional the tangential component of impinging droplets velocity. On the other hand, the

normal component of the velocity is calculated with help from the energy conservation equation:

$$\frac{1}{2}\frac{m_s}{p_a}[U_{s_{N,1}} + ... + U_{s_{N,p_a}}]^2 = E_{K_s} \quad (3.32)$$

where E_{K_s} is the splash kinetic energy due to U_{0_N}.

3.8 Splash Sub-Model Modifications

One of the most important aspects of this study is the reform of the energy equations, so that they consider the effect of crown formation and breaking process. To achieve this goal, as aforementioned, a boundary between corona and prompt splash was established.
Based on Kalantari [29], for the corona splash case , the maximum the non-dimensional crown height (H_c^*) is given as:

$$H_c^* = 0.0039We_n - 0.0354 \quad (3.33)$$

where We_n is the normal Weber number of the impinging droplet. Once We_n is obtained, following the research of Fedorchenko and Wang [25], R_B can be calculated as:

$$R_B \cong 5.68\sqrt{H_c^*} \quad (3.34)$$

Consequently:

$$R_C = R_B + H_C(1 - 4\delta) \quad (3.35)$$

The corona splash process can be described in energy terms by the following formula:

$$E_0 = E_{diss} + E_\sigma + E_{K_s} + E_{\sigma_s} \quad (3.36)$$

where E_0 represents the total incident energy, E_{diss} the dissipation energy , E_σ the surface energy of crown, E_{K_s} the kinetic energy of secondary droplets, and finally E_{σ_s} the surface energy of secondary droplets. These energies can be expressed as:

$$\begin{cases} E_0 = \frac{1}{12}\pi\rho D_0^3 U_0^2 + \sigma\pi D_0^2 \\ E_{diss} = \frac{\pi}{10}\rho U_0^2 D_0 R_B^2 \frac{H_C^*}{\sqrt{Re}} \\ E_\sigma = 2\pi\sigma\delta R_B + 2\sigma(2\pi\frac{R_B+R_C}{2}H_C^*) \\ E_{K_s} = \frac{1}{2}\frac{m_s}{P}\sum_{i=1}^{P} U_i^2 \\ E_{\sigma_s} = \sum_{i=1}^{P}\pi\sigma D_i^2 \end{cases} \quad (3.37)$$

where P is the number of parcels ejected.
The energy equation for the prompt splash is equal to the one presented for the corona splash, with the exception of two of the terms being different:

$$\begin{cases} E_{diss} = \frac{\pi}{270}\rho U_0^2 D_0 \frac{R_P^2 We^{0.477}}{\sqrt{Re}} \\ E_\sigma = \pi\sigma R_P^2 \end{cases} \quad (3.38)$$

In order to establish a comparison order, the sole energy conservation equation present in Ro-

drigues et al. [63] is presented next:

$$E_0 = E_{K_s} + E_{\sigma_s} + E_D \quad (3.39)$$

where:

$$\begin{cases} E_0 = E_{K0} + E\sigma_0 = \frac{1}{2} m_0 U_{0_N}^2 + \pi \rho D_0^2 \\ E_{\sigma_s} = \pi \rho \sum_{i=1}^{P} N_{s,i} D_{s,i}^2 \\ E_D = max(0.8 E_{K_0}; \frac{We_{cr}}{12} \pi \rho D_0^2) \\ E_{K_s} = E_0 - E_{\sigma_s} - E_D \end{cases} \quad (3.40)$$

3.9 Grid Independence

The horizontal velocity component, W , is used to test the grid dependency of the computations. Figure 3.9 shows the vertical profile of the horizontal velocity component at three different planes , $Z = 0.5$,$Z = 1.0$ and $Z = 2.0$, repectively. Two different grids were used. The crossflow velocity at the inlet boundary was used to dimensionless the horizontal velocity component, W. The grid spacing was non-uniform in all directions. As can be observed in figure 3.9, it was found that the improvements obtained with more refined grids are scarce and do not justify the increment of the processing time required for the simulations.

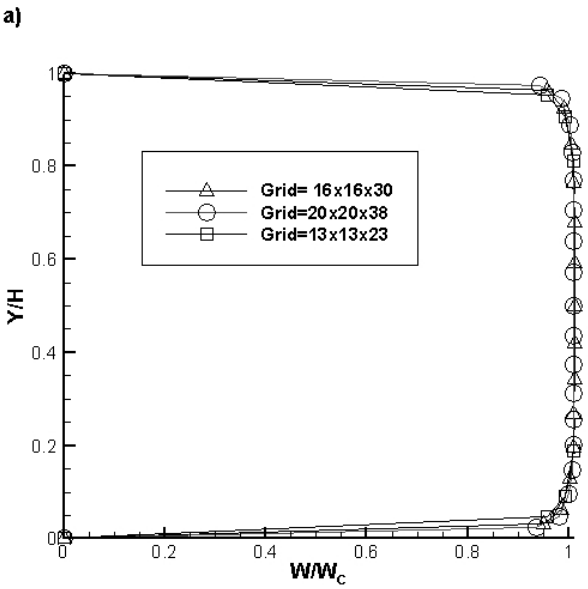

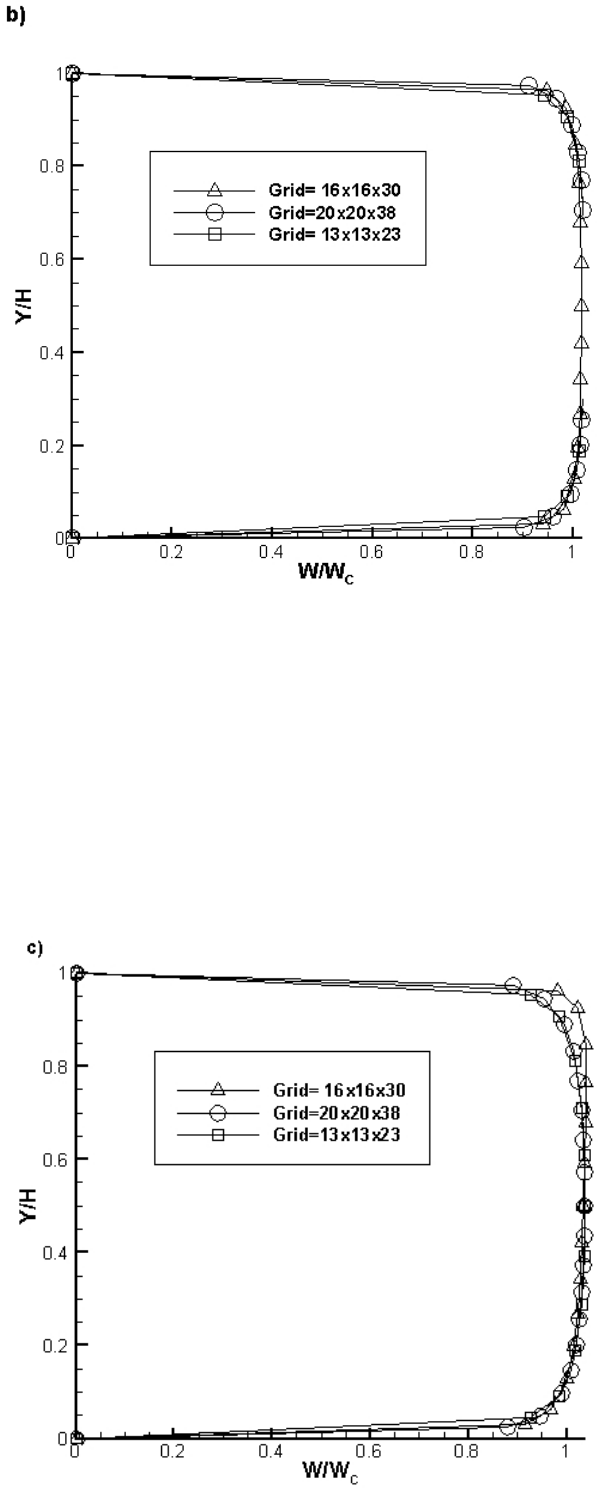

Figure 3.9: Dimensionless vertical profile at, $X/H = 0.5$ of the horizontal velocity component, W. a)$Z = 0.5$, b)=$Z = 1.0$, and c)=$Z = 2.0$.

Chapter 4

Results

From here on out, the obtained results will be presented and there will be given spotlight to the ones related to parameters such as liquid-film distribution, energy dissipation, mass deposition, as well as secondary diameters and velocities. Furthermore, a comparison will be made against the results obtained by Rodrigues et al. [63], in which the same tunnel and impinging conditions apply, although with a different set of impact criteria and secondary atomisation treatment.

4.1 Splash Analysis

4.1.0.1 Splash Distribution

Despite the aforementioned results regarding liquid film deposition, splash distribution analysis corroborates information present in literature in the sense that the temperature rise originates a lot more splashing droplets.
In figures 4.1, 4.2, and 4.3 the downward moving droplets are represented as black circles, and the upward moving ones, resulting from splash or breakup, as light grey. It's important to mention that due to extremely high number of particles depicted , a skip feature of the post-processing software was employed.

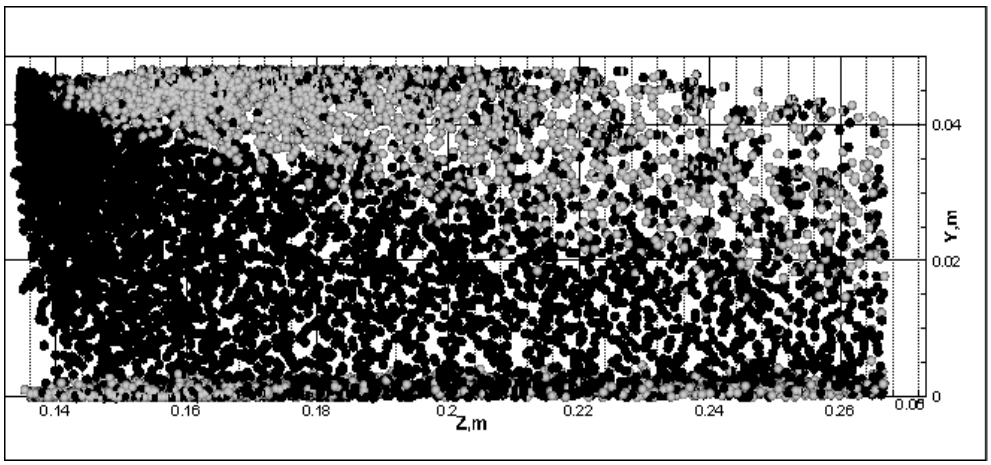

Figure 4.1: Tracking of a full developed spray, where $T = 300K$. New impact criteria and secondary atomisation treatment employed.

When comparing figures 4.1 and 4.2, one can automatically point out the drastic difference between the number of upward moving droplets. This is related with the diferent transition criteria, as aforementioned. Furthermore, there seems to be much more localized and less dispersed zones of upward moving droplets when employing the new impact criteria and secondary atomatization treatment.
Contextualizing, we can see that the intense impingement of smaller droplets produced by splashing between the region of $0.14 \leq Z \leq 0.16$ can be transported and associated with the formation of liquid film in figure 4.6.

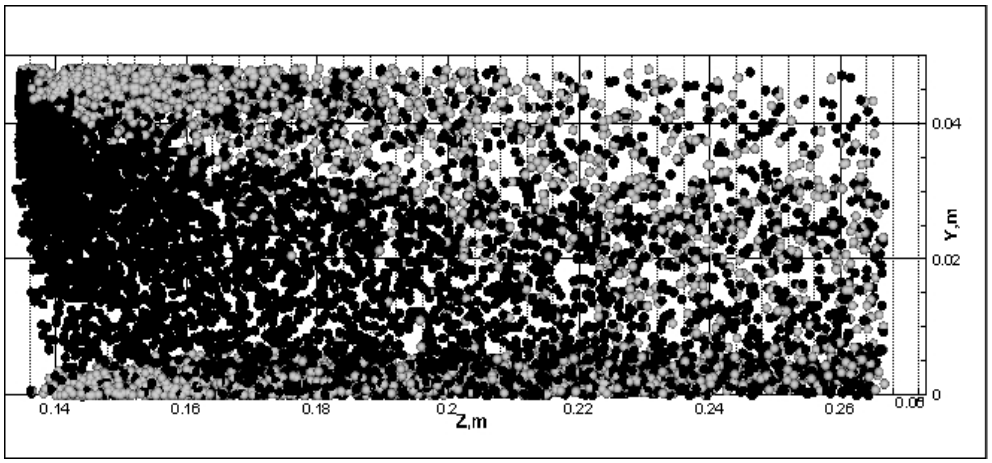

Figure 4.2: Tracking of a full developed spray, where $T = 300K$. Present in Rodrigues et al. [63] .

Another tremendous difference between figures 4.1 and 4.2 is the splash height. This indicates that the drops generated with the new model carry significant less momentum. This is corroborated by the difference found in the values of splash kinetic energy, as depicted in figure 4.4, in which the new model exhibits quite smaller values.
This tendency was also registered in the hotter case tested.

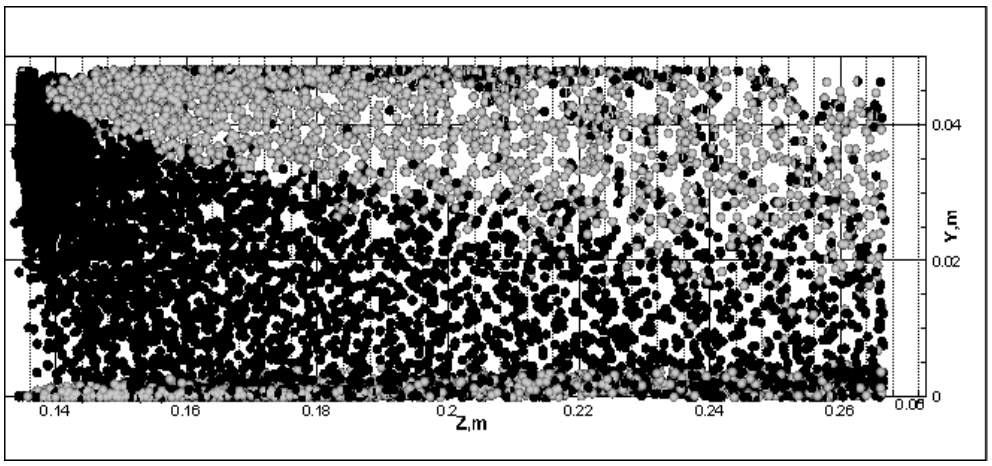

Figure 4.3: Tracking of a full developed spray, where $T = 750K$. New impact criteria and secondary atomisation treatment employed.

Even though lesser upward moving droplets are found in the new model results, the ones present in figure 4.1 ($T = 300K$) are visibly located generally in higher positions regarding the vertical axis when compared with figure 4.3 . This was reported by Cossali et al. [20], where they pointed out that at lower impact velocity the jet height is lower. These results clarify even further the importance of the heat load on the dynamics of impact.

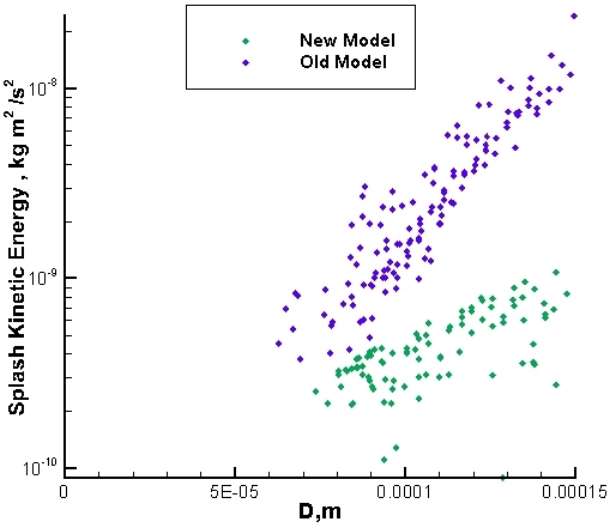

Figure 4.4: Values of splash kinetic energy for different models. $T = 300K$ in both.

4.1.0.2 Secondary Droplets Diameters & Velocities

The knowledge concerning these characteristics of secondary atomisation are of incredible importance to the complete understanding and consequent improvement of processes like spray wall cooling or spray injection in internal combustion engines, since each of them as a different set of needs.

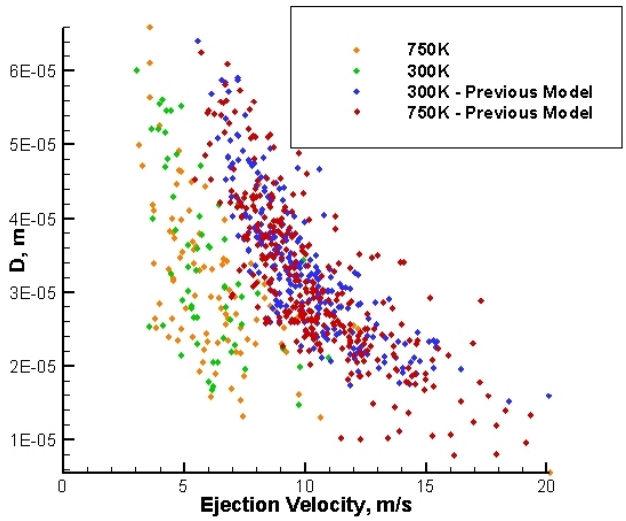

Figure 4.5: Correlation between splashed droplets diameters and ejection velocities. Both models in display.

As expected, the graphs constructed regarding secondary droplets features supported the information aforementioned in this chapter, as smaller secondary atomisation diameters were to be expected due to the diminished impact momentum reported.

This is congruent with the reported observations on morphology by Cossali et al. [20] , in which for both cases ($300K$ and $750K$ that correspond to different heat transfer regimes) a small but consistent decrease of the secondary diameters is registered for impact velocity increase. In its turn, the ejection velocity portrayed in the figure 4.5 is directly dependent of the impact velocity, mainly of its tangential component, as reported by Kalantari [29], which corroborates our result. Morphologically, this is explained by the impact velocity producing an increase of the lamella spreading which results in a decrease of the liquid lamella thickness. Consequently, the lamella thickness influences the secondary drop size.
In comparison with the previously used model , a clear reduction in size and velocity is observed.

4.2 Liquid Film Evolution

When drops impact the surface, they may deposit and consequently form a liquid layer, which, in its turn can influence the behaviour of following impacting particles. In this section, the liquid film distribution is analyzed under the new impact criteria. Results are presented for different temperatures, and then, are compared to the ones presented on Rodrigues et al. [63]. To contextualize, it is important to mention that the splash threshold present in the comparison paper is set at $We_c = 2050La^{-0.183}$ for dry walls, and $We_c = 1320La^{-0.183}$ for wet walls.

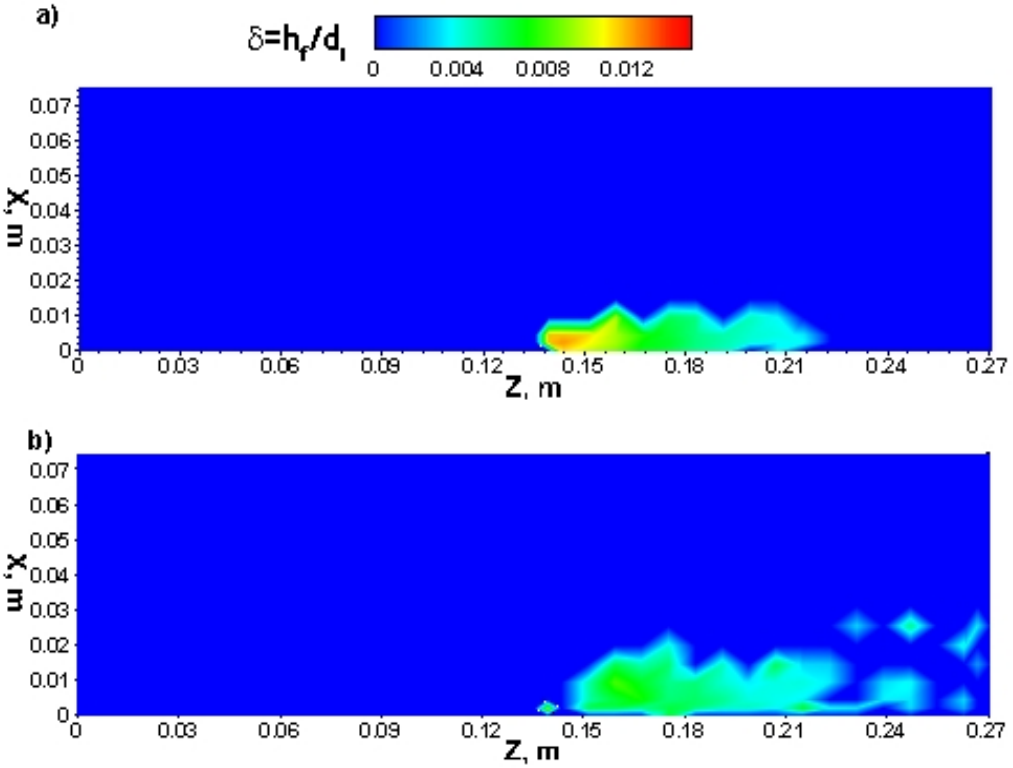

Figure 4.6: Liquid film distributions for $T = 300K$. a) New impact criteria and secondary atomisation treatment employed; b) Employed model presented in Rodrigues et al. [63]

In figure 4.6, we can observe that even at just $300K$ there is a considerable accumulation of liquid film below the injector for the new model. The maximum liquid thickness lies approximately at $Z = 0.14m$. This makes complete sense due to the fact that the deposition/splash

criteria is higher for the new conditions, which leads to a high number of deposited droplets and less spreading downstream due to the decrease of the number of secondary droplets.
Unlike the expected and reported by Rodrigues et al. [63], when the temperature was elevated while employing the new conditions the spray exhibited a less balanced distribution, as shown in figure 4.7. For the hotter case, there is a higher concentration of depositing particles

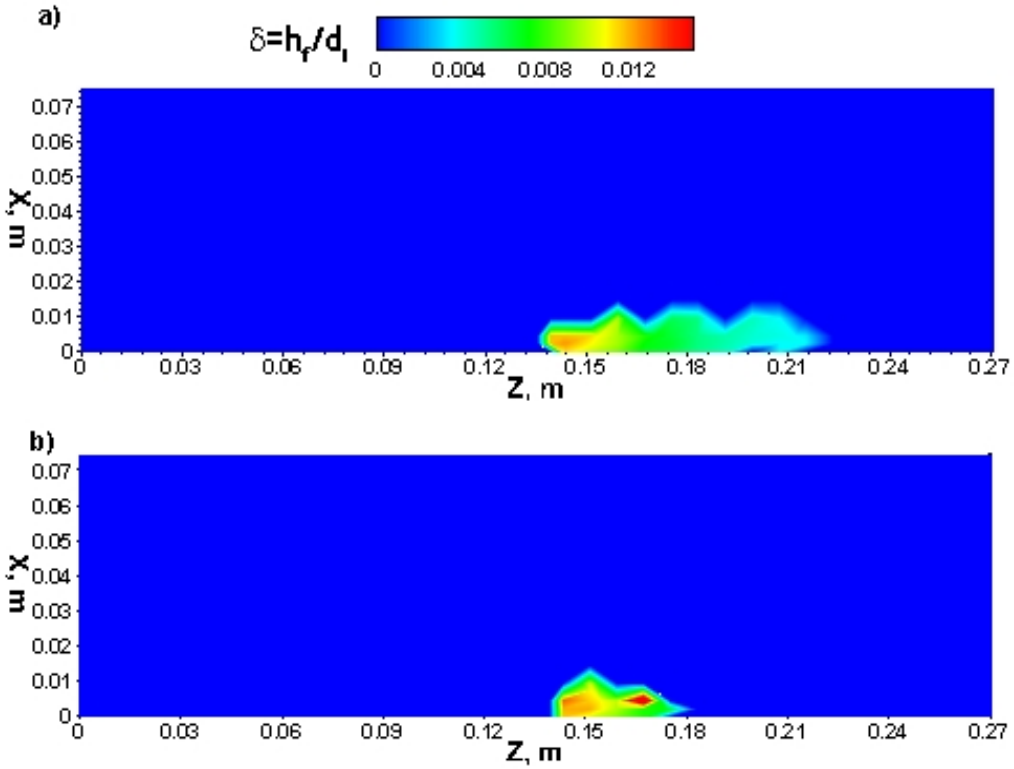

Figure 4.7: Liquid film distributions. a) $T = 300K$; b) $T = 750K$. New impact criteria and secondary atomisation treatment employed on both.

upstream, although it reaches its peak further down, at aproximately $Z = 0.16m$. This temperature exceeds the Leidenfrost point estimated for gasoline, therefore a different behaviour was to be expected. Once the colder droplets ($T = 300K$) are larger, the maximum peak of deposition will happen closer to the injector, as they are less affected by the crossflow. This is evidenced by figure 4.9. Once the wall is wetted, high temperatures will inhibit splash, as the splash transition criteria increases dramatically .
In figure 4.8, the discrepancy in the liquid film deposition location is even bigger that the one presented in figure 4.6. This is explained by the difference of the critical Weber number for hot walls between our new employed criteria and the one present in Rodrigues et al. [63]. A smaller We_{cr} leads to a smaller propagation ratio, once, as we had already established, our secondary atomisation is minor.

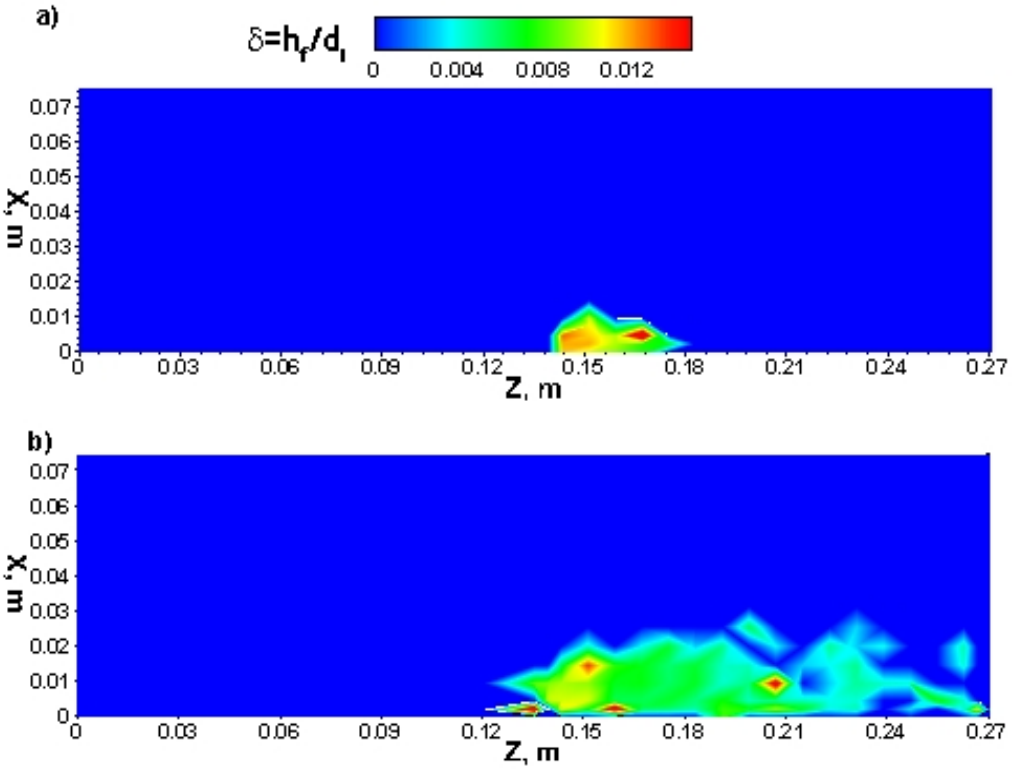

Figure 4.8: Liquid film distributions for 750K. a) New impact criteria employed; b) Employed model presented in Rodrigues et al. [63]

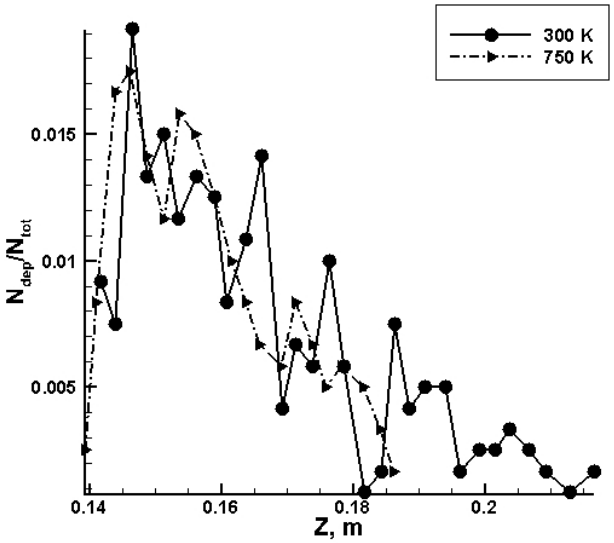

Figure 4.9: Deposited droplets. New impact criteria and secondary atomisation treatment employed.

Chapter 5

Conclusions

The phenomena of spray impact onto solid surfaces, heated or non-heated has a wide spectrum of industrial applications.

This chapter contains the most important conclusions of the implementation of the transition criteria as well as the secondary atomisation treatment presented in Ma et al. [41], Kalantari [29], and Liang et al. [39] in comparison against the model presented in Rodrigues et al. [63].

Spray impingement is a complex phenomenon where several droplet impacts happen based on transient incident and boundary conditions. The model implemented had the advantage of taking into account the distinction between prompt and corona splash in its treatment, which complements in a nice manner the previous work and corresponding simulations, which in its turn translate in a wider range of applications.

Despite being present in the preceding CFD model, the high temperature impact formulation suffered some changes and those reflected in the results, namely when the topic in question was secondary diameters and velocities, and splash distribution. Despite the aforementioned, the treatment of the spray regarding liquid film deposition will require some further studying, as these parameters do not conform one hundred percent with the existing literature. Unlike the results presented in Rodrigues at al. [63], the droplets are not expected to deposit more uniformly in the high temperature case. On the contrary, in high temperature cases when the heat transfer regime in place is film boiling (the wall temperature is higher than the Leidenfrost temperature), the liquid film was shown to deposit in a reduced region.

The new conditions have shown good interpretation of spray properties , such as splash height, under several types of impingement regimes, including the ones under severe temperatures.

Morphology aspects were accounted for and added to the previous model, and incorporated in the energy conservation equations in order to obtain more accurate results regarding the splashing droplets.

The representation of the impinging droplet momentum is in tune with the the theory presented by Cossali et al. [20]: for the film boiling regime the impinging spray has a dwarfish momentum when compared to previous results in Rodrigues et al. [63].

When addressing secondary atomisation diameters and velocities, the achieved results match the ones found in the existing literature , as an increase of impact velocity translates in superior droplet diameters resulting from splash. Even tough the latter statement is true, there is a proportional decrease both in ejection velocities and secondary diameters when compared to the results in Rodrigues et al. [63]. Nevertheless, further investigation is required to explore the presented results and add more detail to the analysis , primarily regarding secondary droplets properties.

The results presented can be relevant to a wide range of applications. In some cases, it's important to lay down a well constituted layer of liquid film, such as in spray painting and spray coating. On the other hand, our results don't seem to be adaptable to fields of study like cooling systems or internal combustion engines, since disintegration of incident drops before impact, as well as uniform distribution, are the technical features that are intended to be registered.

During the evaluation of our results, we concluded that the temperature rise originates smaller

secondary atomatization as well as lesser ejection velocity, which leads to a diminished splash height. Besides that, we could also infer that the droplets were expected to deposit onto the surface less uniformly in high temperature cases, which led to reduced regions of elevated concentration of liquid film. Also, it can be observed that the high wall temperature accelerates the droplet breakup process.

Bibliography

[1] Amsden, A.A., O'Rourke, P.J., Butler, T.D. (1989). *KIVA-II: A computer program for chemically reactive flows with sprays*. United States.

[2] Akhtar, S. Yule, A. (2001). Impaction on a Heated Surface at High Weber Numbers. *ILASS-Europe*, Zurich, Switzerland.

[3] Akhtar, S., Nasr, G. G. Yule, A. J. (2007). Characteristics of water droplet impaction behavior on a polished steel heated surface: Part I *Atom. Sprays, 17*, 659–681.

[4] Bai, C. X. Gosman, A. D. (1995) Development of Methodology for Spray Impingement Simulation. *SAE Technical Paper* 950283, 550–568.

[5] Bai, C. X., Rusche, H. Gosman, A. D. (2002). Modelling of Gasoline Spray Impingement. *Atomization and Sprays* , 12(1-3):1–27.

[6] Barata, J. (1989). *Estudo Numérico e Experimental de Jactos Incidentes Sobre Placas Planas Através de um Escoamento Cruzado*. (PhD thesis, Instituto Superior Técnico).

[7] Bernardin, J. D., Stebbins, C. J. Mudawar, I. (1997). Mapping of impact and heat transfer regimes of water drops impinging on a polished surface. *Int. J. Heat Mass Transfer, 40*(2), 247-267.

[8] Bernardin, J. D., Stebbins, C. J. Mudawar, I. (1997). *Effects of surface roughness on water droplet impact history and heat transfer regime*. Int. J. of Heat and Mass Transfer, 40(1), 73-88.

[9] Bernardin, J. D. Mudawar, I. (1999). A Leidenfrost point model for impinging droplets and sprays. *J. Heat Transfer (Trans. ASME), 126*, 272–278.

[10] Bertola, V. Sefiane, K. (2005). Controlling secondary atomization during drop impact on hot surfaces by polymer additives. *Physics Of Fluids 17*, 108104.

[11] Bertola, V. (2015). An impact regime map for water drops impacting on heated surfaces. *International Journal of Heat and Mass Transfer, 85*, 430–437.

[12] Breitenbach, J., Kissing, J., Roisman, I. V. Tropea, C. (2018). Characterization of secondary droplets during thermal atomization regime. *Experimental Thermal and Fluid Science, 98*, 516–522.

[13] Castanet, G., Liénart, T. Lemoine, F. (2009). Dynamics and temperature of droplets impacting onto a heated wall. *International Journal of Heat and Mass Transfer, 52*, 670–679.

[14] Chen, R. H., Chiu, S. L. Lin, T. H. (2007). *On the collision behaviors of a diesel drop impinging on a hot surface*. Exp. Thermal Fluid Sci., 32(2), 587–595.

[15] Chen, H., Cheng, W., Peng, Y. Jiang, L. (2018). Dynamic Leidenfrost temperature increase of impacting droplets containing high-alcohol surfactant. *International Journal of Heat and Mass Transfer, 118*, 1160–1168.

[16] Chen, H., Cheng, W., Peng, Y. Jiang, L. (2018). Dynamic Leidenfrost temperature increase of impacting droplets containing high-alcohol surfactant. *International Journal of Heat and Mass Transfer, 118*, 1160-1168.

[17] Chiang, C., Yang, T., Casandra, A. Lin, S. (2017). A study of the splash phenomenon of water drops on wood – Emitted droplet velocity and kinetic energy. *Experimental Thermal and Fluid Science, 88*, 444–449.

[18] Cossali, G. E., Coghe, A. Marengo, M. (1997). The impact of a single drop on a wetted solid surface. *Experiments in Fluids, 22,* 463-472.

[19] Cossali, G. E., Marengo, M. Santini, M. (2005). Secondary atomisation produced by single drop vertical impacts onto heated surfaces. *Exp. Therm. Fluid Sci., 29*, 937–946.

[20] Cossali, G. E., Marengo, M. Santini, M. (2008). Thermally induced secondary drop atomisation by single drop impact onto heated surfaces. *International Journal of Heat and Fluid Flow, 29*, 167–177

[21] Crowe, C. T., Schwarzkopf, J. D., Sommerfeld, M. Tsuji, Y. (2012). *Multiphase Flows with Droplets and Particles* (Second edition). Boca Raton, FL: CRC Press,

[22] Deegan, R. D., Brunet, P. Eggers, J. (2008). Complexities of splashing. *Nonlinearity 21*, C1–C11.

[23] Eggers, J., Fontelos, M. A., Josserand, C. Zaleski, S. (2010). Drop dynamics after impact on a solid wall: Theory and simulations. *Physics of Fluids 22*, 062101.

[24] Fard, M., P., Qiao, Y. M., Chandra, S. Mostaghimi, J. (1996). Capillary effects during droplet impact on a solid surface. *Physics of Fluids, 8*, 650.

[25] Fedorchenko, A. I. Wang, A. (2004). On some common features of drop impact on liquid surfaces. *Phys. Fluids 16*, 1349.

[26] Hamdan, K. S., Kim, D. Moon, S. (2015). Droplets behavior impacting on a hot surface above the Leidenfrost temperature. *Annals of Nuclear Energy, 80*, 338–347.

[27] Hobbs, P. V. Osheroff, T. (1967). Splashing of Drops on Shallow Liquids. *Science, New Series, 158,* No. 3805 , 1184-1186.

[28] Huang, Q. Zhang, H. (2008). A study of different fluid droplets impacting on a liquid film. *Petroleum Science*, 5(1):62-66.

[29] Kalantari, D. Characterization of liquid spray impact onto walls and films. *PhD Thesis, Technische Universität, Darmstadt*

[30] Kalantari, D. Tropea, C. Spray impact onto flat and rigid walls: Empirical characterization and modelling. *International Journal of Multiphase Flow*, 33(5):525–544.

[31] Kalantari, D. Tropea, C. (2010). Influence of surface roughness in spray/wall interaction phenomena. *In ILASS - Europe, 23rd Annual Conference on Liquid Atomization and Spray Systems*, 1–6, Brno.

[32] Khana, S., Panuab, R., Bosec, P. K. (2018). Combined effects of piston bowl geometry and spray pattern on mixing, combustion and emissions of a diesel engine: A numerical approach. *Fuel, 225,* 203–217.

[33] Khavari, M., Sun, C., Lohse, D. Tran, T. (2015). Fingering patterns during droplet impact on heated surfaces. *Soft Matter, 11*, 3298–3303.

[34] Kittel, H. M., Roisman, I. V. Tropea, C. (2018). Content of secondary droplets formed by drop impact onto a solid wall wetted by another liquid. *ICLASS 2018, 14th Triennial International Conference on Liquid Atomization and Spray Systems*, Chicago, IL, USA, July 22-26.

[35] Launder, B. E. Spalding, D. B. (1974). The Numerical Computation of Turbulent Flows. *Computer Methods in Applied Mechanics and Engineering, 3*(2), 269–289.

[36] Launder, B. E. Morse, A. (1979). Numerical Prediction of Axisymmetric Free Shear Flows with a Reynolds Stress Closure. *Turbulent Shear Flows,* I, Berlin, Springer-Verlag.

[37] Lee, S. Ryou, H. (2000). Development of a New Spray/Wall Interaction Model. *International Journal of Multiphase Flow, 26*(7), 1209–1234.

[38] Leonard, B. P. (1979). A Stable and Accurate Convective Modeling Procedure Based on Quadratic Upstream Interpolation. *Computer Methods in Applied Mechanics and Engineering, 19*(1), 59–98.

[39] Liang, G., Shen, S., Guo, Y. Zhang, J. (2016). Boiling from liquid drops impact on a heated wall. *Int. J. Heat Mass Transf., 100*, 48–57.

[40] Liang, G. Mudawar, I. (2017). Review of drop impact on heated walls. *Int. J. of Heat and Mass Transfer, 106*, 103–126.

[41] Ma, T., Feng, L., Wang, H., Liu, H. Yao, M. (2017). A numerical study of spray/wall impingement based on droplet impact. *International Journal of Heat and Mass Transfer, 112,* 401-412.

[42] Ma, T. Y., Zhang, F., Liu, H. F. Yao, M. F. (2017). Modeling of droplet/wall interaction based on SPH method. *International Journal of Heat and Mass Transfer, 105*, 296–304.

[43] Marengo, M. Tropea, C. (1999). *Aufprall von Tropfen auf Flüssigkeitsfilme*. Deutsche Forschungsgemeinschaft.

[44] Moita, A. S., Moreira, A. L. N. Roisman, I. V. (2010). Heat transfer during drop impact onto a heated solid surface. *Proc. 14th International Heat Transfer Conference*, Washington DC, USA.

[45] Moreira, A. L N., Moita, A. S., Cossali, E., Marengo, M. Santini, M. (2007). Secondary atomization of water and isooctane drops impinging on tilted heated surfaces. *Exp. Fluids, 43*(2–3), 297–313.

[46] Mundo, C., Sommerfeld, M. Tropea, C. (1998). On the Modeling of Liquid Sprays Impinging on Surfaces. *Atomization and Sprays, 8*(6), 625-652.

[47] Mundo, C., Sommerfeld, M. Tropea, C. (1995). Droplet-wall collisions: experimental studies of the determination and breakup process. *International Journal of Multiphase Flow*, 151-173.

[48] Naber, J.D. Reitz, R. D. (1989). Modeling engine spray/wall impingement. *SAE Trans, 97,* 118-140.

[49] Naber, J. D. Farrell, P. (1993). Hydrodynamics of droplet impingement on a heated surface. *SAE*, 930919.

[50] Nikolopoulos, N., Theodorakakos, A. Bergeles, G. (2007). A numerical investigation of the evaporation process of a liquid droplet impinging onto a hot substrate. *International Journal of Heat and Mass Transfer, 50*, 303–319.

[51] Okawa, T., Shiraishi, T Mori, T. (2008). Effect of Impingement Angle on the Outcome of Single Water Drop Impact Onto a Plane Water Surface. *Experiments in Fluids*, 44(2):331–339.

[52] Palacios, J., Hernández, J., Gómez, P., Zanzi, C. López, J. (2013). Experimental study of splashing patterns and the splashing/deposition threshold in drop impacts onto dry smooth solid surfaces. *Experimental Thermal and Fluid Science 44*, 571–582.

[53] Pan, K. L. Law, C. K. (2007). Dynamics of droplet–film collision. *J. Fluid Mech., 587,* 1–22.

[54] Panão, M., Moreira, A. Durão, D. (2013). Effect of a cross-flow on spray impingement with port fuel injection systems for HCCI engines. *Fuel, 106*, 249–257.

[55] Patankar, S. V. Spalding, D. B. (1972). A Calculation Procedure for Heat, Mass and Momentum Transfer in Three-Dimensional Parabolic Flows. *International Journal of Heat and Mass Transfer,15*(10), 1787–1806.

[56] Rahmati, A. R. Zarareh, A. (2018). Application of a Modified Pseudopotential Lattice Boltzmann Model for Simulation of Splashing Phenomenon. *European Journal of Mechanics / B Fluids*.

[57] Rein, M. (2002) Interactions between Drops and Hot Surfaces. *International Centre for Mechanical Sciences , 456*, Vienna.

[58] Rioboo, R., Tropea, C. Marengo, M. (2001) Outcomes from a drop impact on solid surfaces. *At. Sprays*, 11:155–65.

[59] Rioboo, R., Marengo, M. Tropea, C. (2002). *Evolution of liquid drop impact onto solid, dry surfaces.* Exp. Fluids, 33, 112–24.

[60] Rioboo, R., Bauthier, C., Conti, J., Voue, M. Coninck, J. (2003). Experimental investigation of splash and crown formation during single drop impact on wetted surfaces. *Experiments in Fluids, 35,* 648–652.

[61] Rodrigues, C., Barata, J. Silva, A. (2012). Influence of the energy dissipation in the spray impingement modeling. *50th AIAA Aerospace Sciences Meeting*, Nashville, Tennessee, 1–11, January 9–12.

[62] Rodrigues, C. (2016). *Modelling of Spray-Wall Impingement*. (PhD Thesis, Universidade da Beira Interior).

[63] Rodrigues, C., Barata, J. Silva, A. (2017). On the Modelling of Evaporating Sprays Impinging onto Solid Surfaces. *Journal of Thermophysics and Heat Transfer, 31*(1), 109-119.

[64] Roisman, I. V. Tropea, C. (2005). Fluctuating flow in a liquid layer and secondary spray created by an impacting spray. *Int. J. Multiphase Flow.*

[65] Roisman, I. V., Horvat, K. Tropea, C. (2006). Spray impact: rim transverse instability initiating fingering and splash, and description of a secondary spray. *Phys. Fluids (1994-Present), 18*(10), 102104.

[66] Roisman, I. V. (2009). Inertia dominated drop collisions. II. An analytical solution of the Navier–Stokes equations for a spreading viscous film. *Physics of Fluids 21*, 052104.

[67] Senda, J., Kobayasshi, M., Iwashita, S., Fujimoto, H., Utsunomiya A. Wakatabe, M. (1994). Modelling Diesel Spray Wall Impingement on a Flat Wall. *Society of Automotive Engineers, SAE Paper* 94-1894.

[68] Senda, J., Ohnishi, M., Takahashi, T., Fujimoto, H., Utsunomiya, A. Wakatabe, M. (1999) Measurement and Modeling on Wall-Wetted Fuel Film Profile and Mixture Preparation in Intake Port of SI Engine. *In SAE Technical Paper*, 1–16.

[69] Shirolkar, J. S., Coimbra, C. F. M. McQuay, M. Q. (1996). Fundamental Aspects of Modeling Turbulent Particle Dispersion in Dilute Flows. *Progress in Energy and Combustion Science, 22*(4), 363–399.

[70] Shuen, J. S., Chen, L. D. Faeth, G. M. (1983). Evaluation of a Stochastic-Model of Particle Dispersion in a Turbulent Round Jet. *Aiche Journal, 29*(1), 167-170.

[71] Silva, A. R. R. (2007). *Flow and Heat Transfer Characteristics of Evaporating Impinging Sprays* (PhD Thesis, Universidade da Beira Interior).

[72] Sommerfeld, M. (1998). Analysis of Isothermal and Evaporating Turbulent Sprays by Phase-Doppler Anemometry and Numerical Calculations. *International Journal of Heat and Fluid Flow, 19*(2), 173–186.

[73] Staat, H. J., Tran, T., Geerdink, B., Riboux, G., Sun, C., Gordillo, J. M. Lohse, D. (2015). Phase diagram for droplet impact on superheated surfaces. *J. Fluid Mech, 779*, 3.

[74] Stanton, D. Rutland, C. Modeling Fuel Film Formation and Wall Interaction in Diesel Engines. *In SAE Technical Paper*, 960628.

[75] Stow, C. D. Stainer, R. (1977). The Physical Products of a Splashing Water Drop. *Journal of the Meteorological Society of Japan, 55*(5), 518–531.

[76] Ukiwe, C. Kwok, D. Y. (2005). On the Maximum Spreading Diameter of Impacting Droplets on Well-Prepared Solid Surfaces. *Langmuir, 21*, 666-673.

[77] Wal, R. L. V., Berger, G. M. Mozes, S. D. (2006). Droplets splashing upon films of the same fluid of various depths. *Experiments in Fluids, 40,* 33–52.

[78] Wal, R. V., Berger, G. Moze, S. (2006) The splash/non-splash boundary upon a dry surface and thin fluid film. *Experiments in Fluids*, 40: 53–59.

[79] Wildeman, S.,Visser, C. W., Sun, C. Lohse, D. (2016). On the spreading of impacting drops. *Journal of Fluid Mechanics, 805*, 636-655.

[80] Yao, S. Cai, K. Y. (1988). The Dynamics and Leidenfrost Temperature of Drops Impacting on a Hot Surface at Small Angles. *Experimental Thermal and Fluid Science, 1*, 363-371.

[81] Yarin, A. L. Weiss, D. A. (1995). Impact of drops on solid surfaces: self-similar capillary waves and splashing as a new type of kinematic discontinuity. *J. Fluid Mech, 283*, 141–173.

[82] Zou, J., Wang, P. F., Zhang, T. R., Fu, X. Ruan, X. (2011). Experimental study of a drop bouncing on a liquid surface. *Physics of Fluids* 23, 044101.

Appendix A

Accepted Abstract for the 4th Thermal and Fluid Engineering Conference.

ASTFE
American Society
of Thermal and Fluids Engineers

Proceedings of the 4th Thermal and Fluid Engineering Conference, TFEC
April 14-17, 2019, Westin Las Vegas Hotel & Spa, Las Vegas, NV, USA

TFEC-2019-28427

SUBJECT AREAS: Multiphase Flows (https://www.astfe.org/tfec2019/)

KEYWORDS: Spray impingement, Corona splash, Prompt splash, Liquid film, Hot Wall

TITLE: Modeling of a Spray/Wall Interactions

AUTHORS: Rúben F. T. Ribeiro[1], André R. R. Silva[1*], Jorge M. M. Barata[1]

ADDRESS: [1]Aerospace Sciences Department, University of Beira Interior, Rua Marques Avila e Bolama, 6201-001 Covilhã, Portugal

ABSTRACT:
Spray impingement is an important phenomenon affecting a wide variety of applications. The present work describes an implementation of the spray impingement model based on droplet impact experiments and droplet morphology dynamics: a distinction is made between corona splash and prompt splash. Moreover, a physical model of the crown evolution and a liquid film formation are also considered. Numerical simulations are carried out for predicting the outcome of flows, including liquid film formation, droplet breakup, and spray evaporation. An empirical procedure is used to define the initial spray characteristics, which relies on a comprehensive set of free spray measurements. Both spray and secondary droplet characteristics are evaluated, whereby the numerical results are compared against experimental data to ascertain the prediction capabilities and validate the computational model. The size and velocity of secondary droplets depend strongly on the initial conditions of the spray at the injector exit, as well as the interaction between incident droplets, crossflow, liquid film, evaporation rate, and interposed hot wall. All these parameters are considered in this macroscopic model of the spray/wall interactions. This paper addresses a numerical study on spray-wall interactions, aimed at increasing the capability of the modelling of such flows. A comparison is made with experimental data and spray/wall interaction models already available in literature.

*Corresponding Author: andre@ubi.pt